# Deglacial and Holocene Sea ice and climate dynamics in the Bransfield Strait, Northern Antarctic Peninsula

Maria-Elena Vorrath[1], Juliane Müller[2,3,4], Paola Cárdenas[5], Thomas Opel[2], Sebastian Mieruch[2], Oliver Esper[2], Lester Lembke-Jene[2], Johan Etourneau[6,7], Andrea Vieth-Hillebrand[8], Niko Lahajnar[1], Carina B. Lange[5,9,10,11], Amy Leventer[12], Dimitris Evangelinos[7,13], Carlota Escutia[14], Gesine Mollenhauer[2,3]

[1]University Hamburg, Institute for Geology, Hamburg, Germany

[2]Alfred Wegener Institute, Helmholtz Centre for Polar and Marine Research, Bremerhaven, Germany

[3]MARUM – Center for Marine Environmental Sciences, University of Bremen, Germany

[4]Department of Geosciences, University of Bremen, Germany

[5]Centro de Investigación Dinámica de Ecosistemas Marinos de Altas Latitudes (IDEAL), Universidad Austral de Chile, Valdivia, Chile

[6]EPHE/PSL Research University, France

[7]UMR 5805 EPOC, CNRS, Université de Bordeaux, France

[8]Helmholtz Centre Potsdam GFZ German Research Centre for Geosciences, Potsdam, Germany

[9]Centro Oceanográfico COPAS-Coastal, Universidad de Concepción, Chile

[10]Departamento de Oceanografía, Universidad de Concepción, Chile

[11]Scripps Institution of Oceanography, La Jolla, CA 92037, USA

[12]Department of Earth and Environmental Geosciences, Colgate University, New York, USA

[13]Departament de Dinàmica de la Terra i de l'Oceàn, Universitat de Barcelona, Spain

[14]Instituto Andaluz de Ciencia de la tierra, CSIC-Univ. de Granada, Spain

*Correspondence to*: Juliane Müller, juliane.mueller@awi.de

**Abstract**

The reconstruction of past sea ice distribution in the Southern Ocean is crucial for an improved understanding of ice-ocean-atmosphere feedbacks and the evaluation of Earth system and Antarctic ice sheet models. The Antarctic Peninsula (AP) is experiencing a warming since the start of regular monitoring of the atmospheric temperature in the 1950s. The associated decrease in sea ice cover contrasts the trend of growing sea ice extent in East Antarctica.

To reveal the long-term sea ice history at the Northern Antarctic Peninsula (NAP) under changing climate conditions we examined a marine sediment core from the eastern basin of the Bransfield Strait covering the last Deglacial and the Holocene. For sea ice reconstructions, we focused on the specific sea ice biomarker lipid $IPSO_{25}$, a highly branched isoprenoid (HBI), and sea ice diatoms, whereas a phytoplankton-derived HBI triene ($C_{25:3}$) and warmer open ocean diatom assemblages reflect predominantly ice-free conditions. We further reconstruct ocean temperatures using glycerol dialkyl glycerol tetraether (GDGTs) and diatom assemblages, and compare our sea ice and temperature records with published marine sediment and ice core data. A maximum ice cover is observed during the Antarctic Cold Reversal (13.8 ka - 13 ka BP), while seasonally ice-free conditions permitting (summer) phytoplankton productivity are reconstructed for the late Deglacial and the early Holocene from 13 ka to 8.3 ka BP. An overall decreasing sea ice trend throughout the Middle Holocene coincides with summer ocean warming and increasing phytoplankton productivity. The Late Holocene is characterized by a highly variable winter sea ice concentrations and a sustained decline in the duration and/or concentration of spring sea ice. Overall diverging trends in GDGT-based TEX86L and RI-OH' SOTs are found to be linked to opposing spring and summer insolation trends, respectively.

**Key Words**: Bransfield Strait, Holocene, sea ice cover, $IPSO_{25}$, highly branched isoprenoids, diatoms, GDGTs

# 1    Introduction

Sea ice significantly affects the global climate system through its impact on the atmosphere-ocean exchange of heat and gas, the physical and chemical properties of the water masses, ocean circulation, primary production and biogeochemical cycles (Chisholm, 2000; Vancoppenolle et al., 2013). Sea ice cover limits evaporation, affects precipitation and increases the reflection of solar radiation due to a high albedo (Allison et al., 1982; Butterworth and Miller, 2016; Turner et al., 2017). When sea ice forms, cold and dense brines develop, contributing to the formation of intermediate and deep waters (Nicholls et al., 2009). Importantly, the downwelling of these dense water masses can prevent warm currents from reaching the continental shelf and stimulating basal melt of Antarctic ice shelves, with implications for the stability of ice sheets and global sea level (Cook et al., 2016; Escutia et al., 2019; Etourneau et al., 2019; Hellmer et al., 2012; Huss and Farinotti, 2014). During the spring season, sea ice melting boosts marine primary production by seeding algal cells, releasing nutrients and by promoting ocean stratification and a shallow mixed layer depth (Arrigo et al., 1997; Vernet et al., 2008). In addition, nutrient supply can be locally enhanced by wind-driven upwelling activity along the sea ice edge (Alexander and Niebauer, 1981). Enhanced carbon fixation through this sea ice-stimulated biological pump hence leads to an increase of biological

material transport and organic carbon export to the ocean floor, thus lowering surface $p$CO$_2$ (Han et al., 2019; Kim et al., 2004; Schofield et al., 2018; Wefer et al., 1988).

Since satellite-based sea-ice data became available in 1979, fast and profound changes have been observed both in the Arctic as well as West Antarctica and ascribed to anthropogenic global warming (IPCC, 2021). The Western Antarctic Peninsula (WAP), in particular, is experiencing a rapid warming of the atmosphere (Carrasco et al., 2021; Vaughan et al., 2003) and the ocean (Cook et al., 2016). This is accompanied by rapidly retreating glaciers and ice shelves (Cook et al., 2016; Rignot et al., 2019) and by remarkable loss of sea ice cover in the adjacent seas (Parkinson and Cavalieri, 2012).

For an assessment of the region's past sensitivity to climate change, the deglacial and Holocene climate history of the Antarctic Peninsula (AP) has been studied extensively. The Deglacial, the transition from the Last Glacial Maximum (LGM, Clark et al., 2012) to the Holocene, is characterized by a rapid warming punctuated by a distinct cold event, the so-called Antarctic Cold Reversal (ACR) from 14.7 ka to 13 ka BP (EPICA Community Members, 2004; Mulvaney et al., 2012; Pedro et al., 2016). This drastic cooling of both atmosphere and ocean temperatures in the high Southern latitudes is well reflected in  stable isotope records of Antarctic ice cores and within marine sediments (Blunier and Brook, 2001; Domack et al., 2001; Jouzel et al., 1995; Morigi et al., 2003; Stenni et al., 2001). From the Deglacial towards the Middle Holocene, the Antarctic Peninsula Ice Sheet (APIS) retreated rapidly from the outer shelf to its modern configuration with high melt water discharge (Bentley et al., 2014). Several marine and lacustrine Holocene climate records reveal that the timing of both hydrological and environmental changes was highly variable across the AP (Allen et al., 2010; Ingólfsson et al., 2003; Minzoni et al., 2015; Roseby et al., 2022; Sjunneskog and Taylor, 2002; Totten et al., 2022). An overall consensus, however, is that WAP ocean temperatures were, in comparison to the Deglacial or the Late Holocene, warmer during the Early and Middle Holocene, i.e. between 12 ka and 4 ka BP (Shevenell et al., 2011). In contrast, marine sediment records show multiple different climate patterns for the Late Holocene around the AP, including a continuous Neoglacial cooling (Etourneau et al., 2013).Knowledge of past Southern Ocean sea ice variability is crucial to accurately model climate feedbacks  (Crosta et al., 2022). For periods beyond the satellite era, information on past sea-ice conditions is based on proxies from marine sediments, ice cores (*e.g.* Bracegirdle et al., 2015, 2019; Crosta et al., 2022; Escutia et al., 2019; Thomas et al., 2019), and snow petrel stomach oil deposits (McClymont et al., 2022). At present, most climate models not only fail to reproduce observed sea ice trends of the satellite era; simulated sea ice conditions for both glacial and interglacial periods also often disagree with geological proxies (Roche et al., 2012). Ice-core based sea ice reconstructions primarily use  the concentrations of sea salt sodium (WAIS Divide Project Members, 2015). However, since sea salt aerosols might be overprinted by the highly

91    variable wind direction and meteorological conditions in Antarctica, sea salt records may not sufficiently reflect

92    regional sea ice conditions (Thomas et al., 2019). Although marine sediment records usually have a lower temporal

93    resolution than ice cores, marine proxy reconstructions can resolve regional and - depending on the spatial

94    distribution of sediment cores - large-scale changes in sea ice conditions, as well as sea surface and subsurface

95    ocean temperature, primary productivity and marine ecology (Hillaire-Marcel and de Vernal, 2007). In addition to

96    commonly used geochemical, lithological and microfossil proxies (*e.g.* ice rafted debris (IRD), diatom

97    assemblages, total organic carbon), new approaches focus on specific organic biomarkers - highly branched

98    isoprenoids (HBIs) - as proxies to distinguish between open marine and seasonally sea ice covered environments.

99    The di-unsaturated HBI $IPSO_{25}$ (Ice Proxy for the Southern Ocean, $C_{25:2}$, Belt et al., 2016; Massé et al., 2011) that

100   is produced by sea ice algae and deposited on the ocean floor after the sea ice melt in spring has already been

101   applied in Antarctic sea ice reconstructions (*e.g.* Barbara et al., 2013; Denis et al., 2010; Etourneau et al., 2013).

102   Following the phytoplankton-$IP_{25}$ sea-ice index ($PIP_{25}$) approach for the Arctic (Müller et al., 2011), $IPSO_{25}$ has

103   been combined with phytoplankton-derived HBI trienes and/or sterols to determine the phytoplankton-$IPSO_{25}$ sea

104   ice index $PIPSO_{25}$ (Vorrath et al., 2019), which has been successfully evaluated with recent Antarctic spring sea

105   ice concentrations (Lamping et al., 2021). Other studies applied $PIPSO_{25}$ and examined its potential for sea ice

106   reconstructions over the industrial era (Vorrath et al., 2020) and deglacial and Holocene time intervals in the

107   Amundsen Sea (Lamping et al., 2020). Combining these new molecular proxies with the classical diatom

108   assemblage approach and/or geochemical ice core proxies provides a thorough assessment of past sea ice

109   conditions.

110   Here, we present a marine sediment record covering the past 13.8 ka BP and reconstruct Deglacial and Holocene

111   environmental conditions in the eastern Bransfield Strait at the NAP. Our study is based on a multiproxy approach

112   focusing on the sea ice biomarker $IPSO_{25}$, an open ocean marine phytoplankton biomarker (HBI triene), and on

113   glycerol dialkyl glycerol tetraether lipids (GDGTs) for subsurface ocean temperatures (SOT). Additional estimates

114   of primary productivity, winter sea ice coverage (WSI) and summer sea surface temperature (SSST) come from

115   bulk sediment organic carbon and biogenic silica contents and diatom assemblages using transfer functions,

116   respectively. In an intercomparison, we evaluate the different approaches to reconstruct sea ice conditions and

117   ocean temperatures. We discuss our proxy results in regard of other marine sediment and ice core records providing

118   further insight into the environmental dynamics at the Antarctic Peninsula across the Deglacial and the Holocene.

## 2    Material and Methods

### 2.1 Study Area

The Bransfield Strait is located between the NAP and the South Shetland Islands (SSI; Fig. 1a), comprising a trough (> 2000 m) between a narrow shelf to the north (SSI) and a broad shelf area to the south (AP) (Fig. 1b). The shelf areas were affected by intense ice sheet dynamics during the last glaciation (Canals and Amblas, 2016b; Ingólfsson et al., 2003) leaving ice sheet grounding lines and glacial troughs on the seafloor (Canals et al., 2016; Canals and Amblas, 2016a).

The modern Bransfield Basin is influenced by complex oceanic current systems. Cold (< 0 °C) and relatively salty Weddell Sea Water (WSW) enters from the east, flows alongshore the peninsula and fills the Bransfield Strait basins below 150 m water depth.    In the western part of the Bransfield Strait, the WSW mixes with warmer Bellingshausen Sea Water (BSW; 0 - 50 m water depth) and Circumpolar Deep Water (CDR; 200 - 550 m water depth; Collares et al., 2018; Sangrà et al., 2011, 2017), which are transported in a branch of the Antarctic Circumpolar Current (ACC) over the Anvers Shelf. BSW and WSW form the Peninsula Front that runs parallel to the Antarctic mainland (Sangrà et al., 2011, 2017). The interplay of currents leads to a pronounced pycnoclinte within the upper 20 m of the water column in summer, accompanied by a steep temperature gradient in the upper 100 m, as observed in hydrographic profiles from the Bransfield Basin that show a dominance of WSW below 200 m (see Fig. 1c and Sangrà et al., 2011). Modern sea ice conditions at the core site in the eastern Bransfield Strait are characterized by a mean winter sea ice concentration of ca. 50%, which declines to 18% and less than 2% sea ice concentration during spring and summer, respectively (*cf.* Vorrath et al., 2019). While atmospheric temperatures show a rising trend since the 1950s (Carrasco et al., 2021), ocean temperatures are increasingly influenced by warm water intrusions and higher sea surface temperatures (Martinson and McKee, 2012; Meredith and King, 2005). At the core site, mean annual sea surface temperatures are -0.6 °C with up to 0.8 °C during summer (WOA 18; Boyer et al., 2018; Locarnini et al., 2018).

Primary production in the Bransfield Strait is mainly driven by mixing of water masses at the fronts (Gonçalves-Araujo et al., 2015), mixed layer depth and upwelling (Sangrà et al., 2011), sea ice dynamics (Vernet et al., 2008) and iron availability (Klunder et al., 2014). High concentrations of chlorophyll *a* and diatoms are distributed north of the PF and at the SSI, while lower production and communities of plankton nanoflagellates are found between the Peninsula Front and the WAP (Gonçalves-Araujo et al., 2015). Further, changes in coastal primary production are driven by upwelling, elevated iron availability, as well as the nutrient release and surface water stratification generated by melting sea ice in the austral spring (Vernet et al., 2008). A robust link between marine primary production in surface waters and the sediment composition at the underlying ocean floor is reflected in high

concentrations of total organic carbon (TOC), pigments, sterols and diatoms (Cárdenas et al., 2019), and supported by studies confirming high fluxes of sinking particles (Kim et al., 2004; Wefer et al., 1988). In the study area, particle flux is highly variable with seasonal peaks occurring in late spring, which accounts for 85% of the total flux (Ducklow et al., 2008). Lithologically, the sediments consist mainly of terrigenous silt and clay with varying amounts of diatom mud and ooze, and sand (Cádiz Hernández, 2019; Lamy, 2016; Wu et al., 2019).

## 2.2 Sediment samples and age model

Piston core PS97/072-1 (62° 0.39' S, 56° 3.86' W, 1993 m water depth, 1583 cm in length) was recovered in the eastern Bransfield Strait Basin during R/V *Polarstern* cruise PS97 (Lamy, 2016) (Fig. 1). The sediment is dominated by silt with thin layers of sand, clay, and traces of volcanic ash. Single pebbles are present below 630 cm. The core is disturbed below 1015 cm depth and we only considered samples from above this level for our analyses. Sampling for different analytical approaches was done at the Alfred Wegener Institute (AWI) where the samples were stored frozen in glass vials (for biomarker analysis) and at 4 °C in plastic bags (for micropaleontology).

The age model of core PS97/072-1 is based on radiocarbon dating of eight benthic foraminiferal and mollusk fragments samples with the mini carbon dating system (MICADAS) available at AWI (Mollenhauer et al., 2021). From the conventional $^{14}$C age we subtracted a reservoir age based on modelling by Butzin et al. (2017) and also subtracted an estimated ventilation age of 1200 years to account for the considerable water depth of our site (see table supplement section 1), before we calibrated the ages with the calibration curve IntCal20 (Reimer et al., 2020) to calendar years before present (cal BP) with Calib 7.1 (Stuiver et al., 2018). To estimate the age of the core top, TOC and biogenic opal data of the piston core were matched with data from a multicore from the same sampling site that has been previously dated via $^{210}$Pb (Vorrath et al., 2020; supplement section 2). Ages of sediments below the oldest radiocarbon date (868.5 cm; 12.04 ka BP) were extrapolated assuming a constant sedimentation rate. We applied the Bayesian age modelling tool *hummingage*, a freely available tool developed at AWI that has been successfully applied in previous studies (*e.g.* Ronge et al., 2021). As the lack of age constraints between 12 ka and 6 ka BP may introduce chronological uncertainties, we only focus on overall trends reflected in our data and refrain from detailed allocations of known climatic events in this older time period.

## 2.3 Organic geochemical analyses of piston core PS97/072-1

For the analyses of the bulk organic geochemical composition and biomarkers, 334 sediment samples were freeze-dried and homogenized in an agate mortar. Prior to sediment homogenization, coarse grains were separated using a sieve (5 μm mesh size). Total carbon (C) and nitrogen (N) were measured with a CNS analyzer (Elementar Vario

181  EL III, error of standards and duplicates < 5%). TOC was measured on 0.1 g of acidified samples (500 µl HCl)

182  and determined in a carbon-sulphur determinator (CS-800, ELTRA, standard error < 0.6%). To identify the source

183  of TOC, measurements of stable carbon isotopes of bulk organic matter were done at Universität Hamburg (UHH),

184  Germany, and at Washington State University (WSU), USA. At UHH, the samples were acidified three times with

185  100 µl 1 N HCl and dried on a hotplate. High-temperature combustion was done in an Elementar CHNOS Vario

186  isotope elemental analyser at 950 °C and the analysis was conducted with an Elementar IsoPrime 100 isotope ratio

187  mass spectrometer. We calibrated the pure tank $CO_2$ with the International Atomic Energy Agency reference

188  standards IAEA-CH6 and IAEA-CH7. These and two other standards (IVA Sediment and Sucrose) acted as

189  internal standards in the measurement. The error of continuous standard duplicates was < 0.2‰ and <0.06‰ for

190  sample duplicates. At WSU, 100 mg of freeze-dried sediment samples were used. An elemental analyzer coupled

191  with an Isoprime isotope ratio mass spectrometer (IRMS) was used, with a precision of 0.1‰. The running

192  standard was a protein hydrolysate calibrated against NIST standards. Isotope ratios are expressed in units per mil

193  (‰). $\delta^{13}C$ values are expressed in ‰ against Vienna Pee Dee Belemnite (VPDB).

194  Biogenic opal was estimated on 327 samples following the alkaline extraction procedure described by Mortlock

195  and Froelich (1989), but using 0.5M NaOH as a digestion solution (Müller and Schneider, 1993). Extraction and

196  analysis by molybdate-blue spectrophotometry were conducted at the University of Concepción, Chile. Values are

197  expressed as biogenic opal by multiplying the Si (%) by 2.4 (Mortlock and Froelich, 1989). Opal values could be

198  overestimated by 2 - 2.5% since we did not correct for the release of extractable Si from coexisting clay minerals

199   (Schlüter and Rickert, 1998). Instrumental precision was ±0.5%; error of duplicates ≤ 3%). Details on the

200  methodology used can be found in Cárdenas et al. (2019).

201  The extraction, purification and identification of 137 samples to identify HBIs followed the analytical protocol

202  published e.g. in Belt et al. (2014) and Vorrath et al. (2019). Prior to extraction, 40 µl 7-hexylnonadecane (7-HND;

203  0.0019 µg/µl) and 100 µl $C_{46}$ (0.0098 µg/µl) were added as internal standards. Lipids were extracted using ultra

204  sonication and a mixture of $CH_2Cl_2$:MeOH (v/v 2:1; 6 ml). HBIs and GDGTs were separated by means of open

205  column chromatography using $SiO_2$ as the stationary phase and hexane, and $CH_2Cl_2$:MeOH (v/v 1:1) as eluents.

206  HBIs were analyzed by means of an Agilent 7890B gas chromatograph (30 m DB 1MS column, 0.25 mm diameter,

207  0.250 µm film thickness) coupled to an Agilent 5977B mass spectrometer (MSD, 70 eV constant ionization

208  potential, ion source temperature 230 °C). The initial oven temperature of 60 °C was held for 3 min, ramped to

209  325 °C within 23 min, and was held at 325 °C for 16 min. HBIs were identified *via* comparison of their retention

210  times (IPSO25 and HBI triene with RI 2084DB-1MS and 2046DB-1MS, respectively) and mass spectra with

211  published mass spectra (Belt, 2018) and quantified using the ratio of peak areas of individual HBIs (*m/z* 346; *m/z*

348) and the 7-HND ($m/z$ 266) standard and consideration of instrumental response factors. The error of duplicates was <1.4% for $IPSO_{25}$, <2.6% for HBI trienes. The phytoplankton-$IPSO_{25}$ index ($PIPSO_{25}$) was calculated after Vorrath et al. (2019) as:

$$PIPSO_{25} = \frac{IPSO_{25}}{IPSO_{25}+(c\times phytoplankton\ marker)} \ . \tag{1}$$

The concentrations of the phytoplankton-derived HBI z-triene are at the same level as $IPSO_{25}$ and the c-factor was hence set to 1 (Vorrath et al., 2019). To confirm the sea-ice origin of $IPSO_{25}$, the stable carbon isotope composition of $IPSO_{25}$ was examined in 8 samples (with minimum 50 ng carbon) via GC-irm-MS at the GFZ Potsdam, Germany. The GC (7890N Agilent) equipped with an Ultra1 column (50 m x 0.2 mm diameter, 0.33 µm film thickness) was connected to a DeltaVPlus isotope ratio mass spectrometer through a modified GC-Isolink interface. Each sample was separated chromatographically using a temperature program that started with an oven temperature of 80 °C, which was held for 3 min, ramped to 250 °C with 3 °C per min and then ramped to 320 °C with 5 °C per min and finally reached temperature of 325 °C with a ramp of 1 °C per min and held for 15 min. The organic substances of the GC effluent stream were oxidized to $CO_2$ in the combustion furnace held at 940 °C on a CuO/Ni/Pt catalyst. Samples were measured in duplicate and the standard deviation was ≤0.5 ‰. The quality of the isotope measurements was checked regularly (for each analysis) by measuring different $n$-alkane standards with known isotopic composition of n-C15, n-C20, n-C25 (in equal concentration) and n-C16 to n-C30 (in various concentrations) provided by Campro Scientific, Germany and Arndt Schimmelmann, Indiana University, USA. GDGTs were re-dissolved in 120 µl hexane:isopropanol (v/v 99:1) and filtered through polytetrafluoroethylene filters (0.45 µm in diameter) and analyzed using high performance liquid chromatography (HPLC, Agilent 1200 series HPLC system) coupled to a single quadrupole mass spectrometer (MS, Agilent 6120 MSD) *via* an atmospheric pressure chemical ionization (APCI) interface. The individual GDGTs were separated at 30 °C on a Prevail Cyano column (150 mm x 2.1 mm, 3µm). After injection of the sample (20 µl) it passed a 5 min isocratic elution with mobile phase A (hexane/2-propanol/chloroform; 98:1:1, flow rate 0.2 ml/min). The mobile phase B (hexane/2-propanol/chloroform; 89:10:1) was increased to 100% in two steps: a linear increase to 10% over 20 min followed by an increase to 100% within 10 min. During the measurement, the column was cleaned after 7 min *via* backflush (5 min, flow 0.6 ml/min) and re-equilibrated with solvent A (10 min, flow 0.2 ml/min). The conditions of the APCI were a nebulizer pressure of 50 psi, vaporizer temperature and $N_2$ drying gas temperature 350 °C, flow 5 l/min, capillary voltage 4 kV, and corona current 5 µA. Following Liu et al. (2020), iGDGTs and brGDGTs were detected by selective ion monitoring (SIM) of (M+H$^+$) ions (dwell time 76 ms) using their molecular ions (GDGTs-1 (m/z 1300), GDGTs-2 (m/z 1298), GDGTs-3 (m/z 1296), crenarchaeol (m/z 1292) and GDGTs-Ia (m/z 1022), GDGTs-IIa (m/z 1036), GDGTs-IIIa (m/z 1050)) and quantified in relation to the internal

243 standard C$_{46}$ (*m/z* 744). The hydroxylated GDGTs OH-GDGT-0 (*m/z* 1318), OH-GDGT-1 (*m/z* 1316), and OH-

244 GDGT-2 (*m/z* 1314) were quantified in the scans of their related GDGTs (Fietz et al., 2013). The standard deviation

245 was 0.01 units of TEX$^L_{86}$.

246 Kalanetra et al. (2009) showed that GDGT-producing Thaumarchaeota are abundant in subsurface marine waters

247 in both Arctic and Antarctic regions. As Thaumarchaeota were found between 50 m and 200 m water depth in

248 Antarctica (Kim et al., 2012), temperatures based on GDGTs are suggested to reflect sub-surface waters

249 (Etourneau et al., 2013, 2019). Similarly, also RI-OH' based temperatures in Prydz Bay have been interpreted to

250 reflect subsurface water temperatures (Liu et al., 2020). We therefore consider our results to reflect subsurface

251 ocean temperatures (SOTs). We calculated TEX$^L_{86}$ after Kim et al. (2012) with the *m/z* 1296 (GDGT-3), *m/z* 1298

252 (GDGT-2), *m/z* 1300 (GDGT-1):

253 $$TEX^L_{86} = \log \log \left( \frac{[GDGT-2]}{[GDGT-1]+[GDGT-2]+[GDGT-3]} \right)$$

254 $\qquad$ (2)

255 and calibrated with SOT = 50.8 * TEX$^L_{86}$ + 36.1 (Kim et al., 2012). $\qquad$ (3)

256 For the calculation of temperatures based on hydroxylated GDGTs we followed the approach of Lü et al. (2015)

257 $$RI-OH' = \frac{[OH-GDGT-1]+2\times[OH-GDGT-2]}{[OH-GDGT-0]+[OH-GDGT-1]+[OH-GDGT-2]}$$ $\qquad$ (4)

258 and calibrated it with SOT = (RI-OH' - 0.1) / 0.0382. $\qquad$ (5)

259 For the branched and isoprenoid tetraether (BIT) index for indicating terrestrial organic matter (Hopmans et al.,

260 2004) we used crenarchaeol (m/z 1292) and the branched GDGTs and calculated it as:

261 $$BIT = \frac{[GDGT-Ia]+[GDGT-IIa]+[GDGT-IIIa]}{[Crenarchaeol]+[GDGT-Ia]+[GDGT-IIa]+[GDGT-IIIa]}.$$ $\qquad$ (6)

262

263 **2.4 Diatom analyses**

264 We selected a set of 76 samples for the analysis of diatom assemblages. At first, sampling resolution was every

265 40-50 cm; thereafter, and based on the biogenic opal results, resolution was increased (every 8 cm) at intervals

266 with high variability. Freeze-dried samples (20-120 mg) were treated with hydrogen peroxide and sodium

267 pyrophosphate to remove organic matter and clays, respectively, washed several times with DI water until reaching

268 neutral pH. The treated samples were then settled for six hours in B-Ker2 settling chambers to promote an even

269 distribution of settled particles (Scherer, 1994; Schrader and Gersonde, 1978; Warnock and Scherer, 2015). Once

270 the samples were dry, the quantitative slides were mounted with Norland mounting medium (refraction

271 index=1.56). Diatom valves per slide were counted across traverses (at least 400 valves per slide) using an

272 Axioscop 2 Plus and Olympus BX60 at a magnification of ×1000. The counting procedure and definition of

counting units followed those of Schrader and Gersonde (1978). We performed two sets of counts, with and without *Chaetoceros* resting spores. Diatoms were identified to species or species group level and, if applicable, to variety or form level following the taxonomy described by e.g., Gersonde and Zielinski (2000), Armand and Zielinski (2001), Esper et al. (2010), Esper and Gersonde (2014a, 2014b). Diatom analyses were done by the same investigator at the University of Concepción, Chile, and at Colgate University, USA.

Because diatom distribution in the Southern Ocean is directly associated with the temperature zonation and the frontal systems of the ACC (Cárdenas et al., 2019; Esper et al., 2010; Esper and Gersonde, 2014a, 2014b; Zielinski and Gersonde, 1997), diatom species were grouped into ecological assemblages reflecting i) seasonal sea ice – associated with temperatures -1.8 to 0°C; ii) cold open ocean – associated with the maximum sea-ice extent in winter and temperatures between 1 and 4°C; iii) warmer open ocean – with temperatures between 4 and 14°C, and iv) benthic-epiphytic habitats (Buffen et al., 2007; Cárdenas et al., 2019). Additionally, a group of reworked diatoms was identified (specific group composition is described in detail in supplement section 3). A Spearman principal component analysis (PCA) was applied to the diatom assemblages to differentiate their temporal distribution.

For estimation of winter sea ice (WSI) concentrations, we applied the transfer function MAT-D274/28/4an to the total diatom counts (including Chaetoceros resting spores). The transfer function comprises 274 reference samples with 28 diatom taxa/taxa groups and considers an average of 4 analogues (Esper and Gersonde, 2014a). The analogues refer to surface sediments from the Atlantic, Pacific and western Indian sector of the Southern Ocean. There are 10 analogues from the immediate vicinity of the Antarctic Peninsula. The WSI renders sea ice concentrations in a 1° by 1° grid for the September average of the period 1981 to 2010 (Reynolds et al., 2002, 2007). The threshold between the open ocean and the sea ice covered area is set at 15% of sea ice concentration (Zwally et al., 2002) and the average sea ice edge is defined at 40% (Gersonde et al., 2005; Gloersen et al., 1993). The estimation of summer sea surface temperature (SSST) came from the transfer function IKM-D336/29/3q comprising 336 reference samples (Pacific, Atlantic and Indian Southern Ocean) with 29 diatom taxa and three factors (Esper and Gersonde, 2014b). The calculations for WSI were done with the software R (R Core Team, 2012) using the packages Vegan (Oksanen et al., 2012) and Analogue (Simpson and Oksanen, 2012).

## 3    Results

Based on our age model, sediment core PS97/072-1 covers the last 13.8 ka BP with a mean sedimentation rate of 67 cm/ka and a temporal resolution ranging between 50 and 150 years per sample interval. We note a higher

302    sedimentation rate of 95 cm/ka between 5.5 ka and 3 ka BP and few short intervals of lower (19 cm/ka) and higher

303    (190 cm/ka) sedimentation (Fig. 2).

304    Organic geochemical bulk parameters (TOC, biogenic opal), concentrations of HBIs (IPSO$_{25}$, C$_{25:3}$ HBI triene) and

305    diatom species of warmer open ocean conditions and sea ice assemblages of piston core PS97/072-1 are

306    summarized in Figure 3 (additional data can be found in the supplement section 4). TOC increases from very low

307    values of 0.1 wt% at 13.7 ka BP to an average concentration of ~0.8 wt% between 9.9 ka BP and the top of the

308    core with recurring short-lived minima down to 0.03 wt% during the Middle and Late Holocene (Fig. 3f). Some

309    of these TOC minima occur within thin sandy layers of volcanic ash. Biogenic opal shows a similar pattern with

310    minimum values in the lower part of the record (3.2 wt% at 13.0 ka BP) and increases throughout the Deglacial to

311    Holocene with average values of 30 wt% and a maximum of 54.4 wt% at 5.3 ka BP (Fig. 3e).

312    Between 13.8 ka and 13.4 ka BP, both IPSO$_{25}$ and HBI triene concentrations are close to or below the detection

313    limit (0.1 µg g-1 OC). Throughout the record, the IPSO$_{25}$ concentration ranges between 0.1 to 31.5 µg g$^{-1}$ TOC,

314    while the concentration of the HBI triene ranges between 0.1 and 6.6 µg g$^{-1}$ TOC (Fig. 3). IPSO$_{25}$ is absent before

315    13.5 ka BP and rises rapidly to maximum values of 31.5 µg g$^{-1}$ TOC at 12.8 ka BP. Subsequently, concentrations

316    decrease steadily until 8.5 ka BP and then remain at an average level of ~4 µg g$^{-1}$ TOC with a slightly decreasing

317    trend to 1 µg g$^{-1}$ TOC towards the present and smaller peaks of 10 µg g$^{-1}$ TOC at 6.0 and 3.0 ka BP. Only traces

318    of the HBI triene occur until 13.0 ka BP, while its concentration increases up to 6.6 µg g$^{-1}$ TOC after 8.5 ka BP

319    with large fluctuations of more than 5 µg g$^{-1}$ TOC in the Middle Holocene and from 3.4 ka BP to the present.

320    The diatom composition has two contrasting groups indicating open ocean conditions, a cold water assemblage

321    and a warm water assemblage, and a seasonal sea ice assemblage (Fig. 3; see supplement section 3). Although the

322    group reflecting seasonal sea ice is present throughout the core (mostly >20%), the highest contributions are seen

323    before 13 ka BP and between 10.8 and 9.9 ka BP.  The contribution of the warmer open ocean assemblage is very

324    low in the Deglacial and Early Holocene, rises to highest values in the Middle Holocene and remains around 10%

325    in the Late Holocene. A biplot of a principal component analysis (PCA) shows the relationship of the ecological

326    groups for three time intervals with clear dominance of seasonal sea ice before 13 ka BP and warmer open ocean

327    conditions after 8.5 ka BP (supplement section 5 and 6).

328    Sea ice concentration estimates based on diatom assemblages (WSI) and the PIPSO$_{25}$ index as well as the content

329    of IRD in PS97/072-1 are summarized in figure 4 (a-c). Reconstructed winter sea ice concentrations (% WSI)

330    derived from the MAT transfer function  range from 80% to 90% during the ACR and the Deglacial (13.8 ka – 11

331    ka BP) and exhibit an overall decreasing trend over the Middle Holocene with fluctuations reaching minimum sea

332    ice concentrations of ca. 65% during the Middle and Late Holocene (Fig. 4a). PIPSO$_{25}$ values show a similar trend

indicating higher sea ice cover during the ACR, the Deglacial and the Early Holocene ($PIPSO_{25} > 0.8$) and a successive decline to 0.5 on average throughout the Middle and Late Holocene with a distinct minimum at 0.5 ka BP (Fig. 4b). IRD (lithic particles and pebbles > 5 µm) occurs frequently between 13.8 ka and 9 ka BP and is virtually absent in the younger part of the sediment core (Fig. 4c).

Figure 5 provides ocean temperature anomalies based on diatom assemblages (SSST) and GDGT-derived RI-OH' and $TEX_{86}^L$ SOTs in core PS97/072-1 (Fig. 5 b-d). Diatom-derived SSST estimates generally depict lower temperatures during the Deglacial and Early Holocene, accompanied by a shift to ca. 1 °C warmer temperatures in the Middle and Late Holocene (Fig. 5b). A short cold event with a SSST decrease of ca. 1.5 °C occurred around 3.1 ka BP. Similar to SSSTs, RI-OH'-derived SOTs likewise reflect generally lower temperatures during the Deglacial and Early Holocene, and 0.4 °C warmer temperatures in the Middle and Late Holocene (Fig. 5c). $TEX_{86}^L$-derived SOTs display an opposite trend to both SSST and RI-OH' SOT with peak temperatures during the Deglacial and an overall Holocene cooling towards present (Fig. 5e).

## 4    Discussion

### 4.1 The late Deglacial (13.8 ka to 11.7 ka BP)

In the oldest part of our sediment record, covering the later part of the last Deglacial from 13.8 ka until 11.7 ka BP, we observe a remarkable environmental change indicated by large shifts in the TOC, biomarker and diatom records (Fig. 3). The very low concentrations of HBIs (Fig. 3b and d), TOC (Fig. 3f), and biogenic opal (Fig. 3e) between 13.8 ka and 13.5 ka BP suggest that primary production of phytoplankton and also sea ice algae synthesizing $IPSO_{25}$ was diminished, while sea ice related diatom species show the highest contribution of 73% (Fig. 3c), albeit with very low concentrations (see online ressource). Highest WSI concentrations and PIPSO25 values   (Fig. 4a, b) are pointing towards a maximum sea ice cover and are well in line with peak ssNa concentrations in the EDML and WAIS ice core records, referring to an extended sea ice cover until 13 ka BP (Fig. 4; EPICA Community Members, 2006; Fischer et al., 2007; WAIS Divide Project Members, 2015). We note that for the interpretation of $PIPSO_{25}$ values, changes in both $IPSO_{25}$ and HBI triene concentrations need to be evaluated carefully to reliably deduce information on sea ice conditions. High $PIPSO_{25}$ values may refer to an extended sea ice cover that lasts until summer (thus hampering phytoplankton productivity/HBI triene synthesis), whereas low $PIPSO_{25}$ values point to a reduced sea ice cover in terms of duration (in spring) and/or sea ice concentration.  The near absence of $IPSO_{25}$, the HBI triene and warm open ocean diatom species between 13.8 ka and 13.5 ka BP evidences a permanent, potentially perennial ice cover or at least sea ice that was too thick to allow

photosynthesis of sea ice algae inhabiting the sea ice. Similarly, Lamping et al. (2020) related the absence of IPSO$_{25}$ and phytoplankton-derived dinosterol in sediments in the western Amundsen Sea to the re-advance of a floating ice shelf canopy during the ACR. At the PS97/072-1 core site in the eastern Bransfield Strait, both the presence of perennial sea ice, or an ice shelf tongue extending from the APIS, could explain the lack of indicators of phytoplankton productivity and IPSO$_{25}$-synthesizing ice algae. We hence assume that the very low absolute concentrations of sea ice-associated diatoms result from lateral transport underneath the ice or reworking of sediments older than 13.5 ka BP. The abrupt increase in IPSO$_{25}$ concentrations at 13.5 ka BP may indicate the retreat or thinning of such an ice-canopy, permitting sea ice algae growth during spring and a subsequent increase in primary production reflected in rapidly rising HBI triene concentrations since 13 ka BP (Fig. 3b, d). Such a transition from a perennial floating ice canopy to conditions characterized by (seasonal) sea ice cover is also reported by Milliken et al. (2009)for the nearby Maxwell Bay (King George Island; SSI) between 14 ka and 10 ka BP. Interestingly, a prominent decrease in sea ice associated diatoms between 13 ka and 12 ka BP (Fig. 3c) is not mirrored by the still high WSI concentrations. This discrepancy could relate to a weaker preservation potential of certain diatoms reflecting seasonal sea ice (e.g. Synedropsis sp., Nitzschia stellata) that are not considered within the transfer function to estimate WSI, which highlights the need to examine silica dissolution effects for the interpretation of diatom records.

With regard to the ocean temperatures recorded at core site PS97/072-1, we note that the overall cool deglacial temperatures derived from diatom data (SSST) and hydroxylated GDGTs (RI-OH') seem to be linked to the lowered summer insolation (Fig. 5a), whereas higher TEX$_{86}^{L}$ temperatures seem to be associated with a higher spring insolation (Fig. 5d). While the impact of seasonality on GDGT-based ocean temperature estimates is still under debate and would require further improvements in regional calibration, the observation of maximum abundances of thaumarchaeota species (producing isoGDGTs applied to determine TEX$_{86}^{L}$) in Antarctic coastal waters during spring (Kalanetra et al., 2009; Murray et al., 1998) seems to support our interpretation and also helps to explain the divergent trends in TEX$_{86}^{L}$ and RI-OH' derived SOT estimates, as the latter proxy might be also sourced by other archaea species that probably grow mostly during the summer season.

While the ACR lasts from 14.7 ka to 13 ka BP (Pedro et al., 2016) as indicated by e.g. the WAIS Divide ice core records (Fig. 5i, WAIS Divide Project Members, 2013), our sediment record shows that cold conditions with an extended sea ice cover, limiting summer phytoplankton productivity (Fig. 4a, b) in the eastern Bransfield Strait, lasted until ca. 11 ka BP. Further, the Deglacial and Early Holocene IRD content (Fig. 4.c; including the presence of single large pebbles) in core PS97/072-1 points to the frequent occurrence of icebergs, evidencing the overall ice sheet disintegration along the WAP that occurred around 14 ka BP at the SSI and promoted seasonally open-

marine conditions at Anvers-Hugo Trough at 13.6 ka BP (middle WAP shelf) and at 12.9 ka BP in Palmer Deep (inner WAP shelf), respectively (Domack et al., 2001; Domack, 2002; Jones et al., 2022; Milliken et al., 2009; Roseby et al., 2022). At our core site, rising RI-OH' SOTs and a slight decrease in PIPSO$_{25}$ values characterize the late Deglacial between 13 ka and 11.7 ka BP (Fig. 4b, 5c). A prominent decline in large-scale sea ice cover is also reflected in the decreasing ssNA concentrations in the EDML and WAIS ice cores between 13 ka and 11.7 ka BP (Fig. 4e, f) likely related to a distinct atmospheric warming, as reflected in ice core stable water isotopes (Fig. 5h).

The ACR cooling and the subsequent Late Deglacial warming may relate to inter-hemispheric teleconnections through a global reorganization of atmospheric and ocean circulation that is associated with the bipolar seesaw pattern of opposite climate trends between the northern and southern hemisphere (Anderson et al., 2009; Broecker, 1998; EPICA Community Members, 2006; Pedro et al., 2016). While a northward shift of the southern westerlies during the ACR (Fletcher et al., 2021) promoted Antarctic sea ice expansion and glacier readvance (potentially causing an ice cover over the PS97/072-1 core site), a cooling of the northern hemisphere with a southward shift of the Intertropical Convergence Zone and the southern hemisphere westerlies (Lamy et al., 2007) resulted in intensified wind stress in the Drake Passage (Timmermann et al., 2007). This pattern would have increased upwelling that may have driven the continued ocean warming and sea ice retreat in Antarctica towards the Holocene (Anderson et al., 2009).

**4.2 Early Holocene warming from 11.7 ka to 8.2 ka BP**

The Early Holocene from 11.7 ka to 8.2 ka BP is characterized by a progressively decreasing spring sea ice cover inferred from declining PIPSO$_{25}$ values (Fig. 4b), as well as highly variable winter sea ice cover with prominent shifts in sea ice concentration (from 90% to 65%; Fig. 4a). These WSI fluctuations are not reflected in the sea ice diatom assemblage, which, similar to the biogenic opal content, follows an increasing trend until 10.5 ka BP (Fig. 3c, e). Increased accumulation of biogenic opal and a better preservation of (thin-walled) sea ice-related diatoms that are not used for the transfer function may explain the mismatch between the WSI record and sea ice diatom assemblage. The increase in biogenic opal is further accompanied by rising TOC content, while concentrations of the HBI triene and warm open ocean diatoms remain low, only an increase after 9 ka BP, signalling higher phytoplankton productivity (Fig. 3a, b). Diatom-derived SSSTs exhibit marked fluctuations but remain relatively low until 8.2 ka BP (Fig. 5b). RI-OH' and TEX$_{86}^{L}$ SOTs display diverging trends following the summer and spring insolation, respectively (Fig. 5). While PIPSO$_{25}$ values display a gradual decrease in sea ice coverage, the WSI record suggests a highly variable sea ice cover, with several distinct sea ice minima between 11 ka and 10 ka BP

and around 9 ka BP (Fig. 4a and b). These sea ice minima may have resulted from punctuated warming events, *e.g.* around 10 ka BP, when SSST shows a short temperature peak, which might have led to a delayed sea ice formation in autumn and winter (Fig. 5b). Another WSI minimum at 9 ka BP coincides with a major, final peak in IRD deposition at the core site (Fig. 4), evidencing iceberg discharge during episodes of peak AP ice-sheet retreat and enhanced calving (Jones et al., 2022). As sea ice melting may have been an important driver of ocean stratification, we suggest warmer, stratified surface waters with moderate production in summer, supported by increasing summer insolation (Fig. 5a). Ameliorating climate conditions, ice-shelf retreat along the NAP and the establishment of modern-like ocean conditions after 9 ka BP have also been proposed for the western Bransfield Strait by Heroy et al. (2008)and are well in line with the rising concentrations of warm open ocean diatoms and the phytoplankton-derived HBI triene at our core site after 9 ka BP (Fig. 3). The general decrease in spring sea ice cover (reflected in declining $PIPSO_{25}$ values) may have been fostered by a maximum spring and rising summer insolation (Fig. 5a, d), shortening the duration of sea ice cover. Rising RI-OH' temperatures are consistent with the overall slight warming trend recorded in the WAIS Divide ice core (Fig. 5h), which has been shown to be mainly driven by increasing summer temperatures (Jones et al., 2022). The decreasing $TEX_{86}^L$ SOT trend at core site PS97/072-1 corresponds to the declining $TEX_{86}$ temperatures reported for ODP site 1098 in Palmer Deep (Fig. 5g; Shevenell et al., 2011) though the latter displays a more pronounced temperature drop (of ca. 6 °C) between 11.7 ka and 8.2 ka BP. These regional differences may relate to changing ocean circulation patterns, associated shifts in water mass distribution along the WAP and the local post-glacial environmental development during the Early Holocene. Deposition of laminated diatom oozes in the Anvers-Hugo Trough at the WAP middle shelf during the early Holocene, *e.g.*, documents episodes of extremely high productivity in response to a southward shift of the southern hemisphere westerlies and the advection of warm and nutrient-rich CDW (Roseby et al., 2022). We propose that the eastern Bransfield Strait remained mainly "inaccessible" for CDW and BSW until further ice recession between 10 ka and 5 ka BP (Ó Cofaigh et al., 2014 and references therein) permitted advection of these water masses into the Bransfield Strait.

**4.3 Middle Holocene from 8.2 ka until 4.2 ka BP**

The Middle Holocene from 8.2 ka to 4.2 ka BP was a period of sea ice retreat and minimum iceberg activity at the core site indicated by decreasing WSI and $PIPSO_{25}$ values and virtually absent IRD (Fig. 4). Diatoms associated with warmer open ocean conditions, peak HBI triene concentrations and maximum TOC as well as biogenic opal contents (Fig. 3) indicate a high export production during the Middle Holocene. This higher primary productivity can be linked to a decrease in both winter and spring sea ice indicated by WSI and $PIPSO_{25}$ minima, respectively

456    (Fig. 4a, b), elevated SSSTs and (summer) SOTs (Fig. 5b, c) promoting ice-free summer ocean conditions

457    favorable for phytoplankton productivity. These Middle Holocene sea-ice conditions compare well with modern

458    situation at the core site characterized by a seasonal decrease in sea ice concentration from 50% during winter to

459    mainly ice-free summers (NSIDC; Cavalieri et al., 1996).

460    The continued retreat of the previously grounded APIS adjacent to the Bransfield Strait between 10 ka and 5 ka

461    BP finally opened the passage for ACC waters to enter the Bransfield Strait from the west (Bentley et al., 2014; Ó

462    Cofaigh et al., 2014). As a result, we suggest that sea ice conditions at our core site were influenced by incursions

463    of warmer ocean waters carried with the ACC (i.e. BSW and CDW), while cold water inflow and sea ice advection

464    from the Weddell Sea was diminished due to the still grounded ice sheet at the tip of the AP (Ó Cofaigh et al.,

465    2014), leading to a shorter sea ice season in the eastern Bransfield Strait. This shift towards a warmer, less ice-

466    covered ocean setting in the eastern Bransfield Strait is reflected in the transition from proximal to distal

467    glacimarine conditions in Maxwell Bay (Milliken et al., 2009) and may be associated with the Mid-Holocene

468    climatic optimum. This timing contrasts the notion of Heroy et al. (2008), who, confined the Mid-Holocene

469    climatic optimum to a shorter time interval between 6.8 ka and 5.9 ka BP based on diatom assemblage analyses of

470    a sediment core in the western Bransfield Strait. We propose that this temporal offset may relate to regionally

471    different responses, glacial retreat patterns impacting oceanic pathways and the position of frontal systems

472    controlling primary productivity within Bransfield Strait. The generally decreasing WSI and variable $PIPSO_{25}$

473    values further depict different trends than $PIPSO_{25}$ values determined for the JPC10 in Palmer Deep ( Fig. 4d;

474    Etourneau et al., 2013), which suggest an overall increase in spring sea ice along the WAP until 4.2 ka BP. Though

475    minima in spring sea ice at 7.5 ka, 6.5 ka and 5.4 ka BP at core site PS97/072-1 may be related to $PIPSO_{25}$ minima

476    observed for JPC10, the lack of Middle Holocene age tie points in our core from the Bransfield Strait prevents us

477    from concluding on a common driver for these sea ice reductions.

478    Regarding ocean temperatures, we observe a sustained warming in RI-OH' SOT, punctuated by a cooling at 5.5

479    ka BP (Fig. 5c), while $TEX_{86}^{L}$ temperatures depict a subtle cooling of ca. 0.5 °C between 8.2 ka and 7 ka BP,

480    followed by a warm reversal until 6 ka BP, and a further cooling until 4.2 ka BP (Fig. 5e). This Middle Holocene

481    slight cooling trend is also observed in the $TEX_{86}^{L}$ records from the core sites in Palmer Deep at the WAP ( Fig.

482    5f, g; Etourneau et al., 2013; Shevenell et al., 2011). The similarity between these records encourages us to assume

483    that these $TEX_{86}$-derived temperatures from along the WAP and NAP are driven by spring insolation rather than

484    being a reflection of annual mean ocean temperature conditions.

**4.4 Late Holocene and Neoglacial from 4.2 ka BP until today**

The Late Holocene covering the past 4.2 ka BP is characterized by a highly variable winter sea ice and decreasing spring sea ice cover at core site PS97/072-1, as indicated in the MAT-derived WSI and a decline in $PIPSO_{25}$ values over the past 2 ka (Fig. 4a, b). Rather constant biogenic opal and TOC contents (Fig. 3e, f), however, suggest that primary productivity remained relatively unaffected by this reduction in spring sea ice cover. While decreasing $IPSO_{25}$ concentrations between 2.5 ka BP and the core top (Fig. 3d) suggest a reduced productivity of the sea ice diatom species synthesizing this molecule, no significant changes are observed in the sea ice diatom assemblage (Fig. 3c), which supports the assumption that only a restricted group of diatoms - at least *Berkeleya adeliensis* - produce $IPSO_{25}$ (Belt et al., 2016). The warm open ocean diatom assemblage follows an overall declining trend throughout the Late Holocene, which is not reflected in the highly variable and slightly increasing HBI triene concentrations (Fig. 3a, b), and a prominent decrease in HBI triene concentrations occurs only at 1 ka BP. While the observation of cooler sea surface temperatures, and a diminished spring sea ice cover indicated by the joint decrease in the warm open ocean diatom assemblage and $PIPSO_{25}$ values since 2 ka BP may seem counterintuitive, Milliken et al. (2009) report a similar development in Maxwell Bay since 2.6 ka BP. Interestingly, records of diatom and radiolarian assemblages of a sediment core (Gebra-2) collected in close vicinity to PS97/072-1 document an overall increase in sea-ice taxa over the past 3 ka BP with distinct Neoglacial events characterized by higher (denser and longer) sea ice cover (Bárcena et al., 1998). The lower sampling resolution and missing age control for the past 3 ka BP in PS97/072-1, however, hamper a more detailed comparison of diatom species in our core with those investigated for Gebra-2. The Neoglacial increase in spring sea ice cover is also indicated by a prominent rise of $PIPSO_{25}$ values determined for JPC10 in Palmer Deep (Fig. 4d; Etourneau et al., 2013). Similarly, deposition of ssNa in the EDML ice core (Fischer et al., 2007) increases since 2 ka BP.

Minimum PS97/072-1 $PIPSO_{25}$ values at 0.5 ka BP result from notably reduced $IPSO_{25}$ and HBI triene concentrations (Fig. 3b, d). While this pattern of minimum HBI triene and $IPSO_{25}$ concentrations is similar to the period between 13.8 ka and 13.5 ka BP, which was characterized by cold conditions and a pronounced - potentially perennial - ice cover, the elevated TOC and biogenic opal values, as well as the presence of diatoms associated with warm open ocean conditions at 0.5 ka BP, point to favorable ocean conditions. We hence relate this drop in HBI concentrations to a shift in the diatom community rather than to an abrupt readvance of an ice cover.

Late Holocene ocean temperature reconstructions for core PS97/072-1 display different patterns. Generally increasing diatom-derived SSSTs are only punctuated by a cooling event at 3.1 ka BP, while RI-OH' SOT remains relatively constant with a very subtle cooling of ca. 0.2 °C between 1.5 ka and the present, which could be linked to the slight decrease in summer insolation (Fig. 5a, b, c). The decrease in $TEX_{86}^L$ SOT by about 1 °C between 4

ka and 3.3 ka BP in eastern Bransfield Strait is also depicted in the TEX$_{86}^L$ data from the Palmer Deep core JPC10 (Fig. 5e, f; Etourneau et al., 2013). The following warming reflected in PS97/072-1 TEX$_{86}^L$ SOT until ca. 2 ka BP may relate to the establishment of open marine conditions fostering primary productivity at the Perseverance Drift north of Joinville Island (northern tip of the AP) as a result of warm water intrusions (Kyrmanidou et al., 2018). This warming is reversed by another cooling at about 2 ka BP - coincident with an abrupt temperature increase of ca. 4 °C depicted in the ODP1089 TEX$_{86}$ SOT record in Palmer Deep (Fig. 5g; Shevenell et al., 2011). The latter warming is not displayed in the TEX$_{86}^L$ data of the nearby JPC10 and we relate this contrast to the different approaches used to determine SOT (*i.e.*, TEX$_{86}$ vs. TEX$_{86}^L$ omitting the crenarchaeol regio-isomer, which seems to be less important for membrane adaptation in polar waters; Kim et al., 2010).

Evidently, temperature trends at the AP in the Late Holocene are highly variable between different areas (Allen et al., 2010; Barbara et al., 2016; Bárcena et al., 1998; Bentley et al., 2009; Etourneau et al., 2013; Mulvaney et al., 2012; Shevenell et al., 2011) and this is likely associated with the complex oceanographic and atmospheric settings. This heterogeneous pattern, however, contrasts with the currently observed large-scale ocean warming along the AP driven by intrusions of ACC-derived warm CDW onto the continental shelf of the WAP (Couto et al., 2017) and the NAP (Ruiz Barlett et al., 2018), as well as the overall loss of sea ice (Parkinson and Cavalieri, 2012), which supports the assumption that the changes impacting the AP already exceed natural variability.

## 5    Conclusions

We reconstructed the sea ice and climate development at the NAP since the last Deglacial using the sediment core PS97/072-1 from the eastern Bransfield Strait. Pursuing a multi-proxy approach that focuses on organic geochemical bulk and biomarker analyses, diatom assemblage studies and transfer functions as well as IRD data, we identified different Deglacial and Holocene environmental conditions impacted by sea ice and ocean temperature changes. Our results reveal the retreat of a perennial ice cover after the ACR and an overall sea ice reduction and warming summer ocean temperatures during the Holocene. The late Deglacial from 13.8 ka to 11.7 ka BP was a highly dynamic period: until 13.4 ka BP primary productivity was diminished due to a permanent ice cover during the ACR. The ACR terminated with a shift to slightly warming conditions at 13 ka BP along with a reduction in the length of the sea ice season, which permitted phytoplankton productivity at least during summer. The Early Holocene from 11.7 ka to 8.2 ka BP was characterized by increasing summer ocean temperatures, further decreasing sea ice cover in terms of duration and/or sea ice concentration and highly variable winter sea ice cover. In the Middle Holocene from 8.2 ka to 4.2 ka BP, increased advection of BSW and CDW led to a shortened sea

546 ice season confined to winter and spring and rising summer ocean temperatures fostering primary production,

547 indicating the Middle Holocene Climatic Optimum. During the Late Holocene, the core site experienced distinct

548 fluctuations in WSI with concentrations shifting between 90% and 60%, while PIPSO$_{25}$ values declined

549 continuously suggesting a less intensive or shorter spring sea ice cover. We note that GDGT-based TEX$_{86}^{L}$ and

550 RI-OH' SOTs correspond to spring and summer insolation, respectively, which may explain the divergent trends

551 displayed by both SOT proxies. Clearly, while this observation may help with the interpretation of other Southern

552 Ocean GDGT-based temperature estimates and the reconstruction of seasonal SOT variability, more investigations

553 into the mechanisms driving GDGT synthesis in polar waters are needed.

554

**Data Availability**

All data mentioned in this paper will be available at the open access repository www.pangaea.de (https://doi.pangaea.de/10.1594/PANGAEA.952279).

**Author contributions**

The study was conceived by MV and JM. Data collections and experimental investigations were done by MV together with CBL (core description, sampling, diatoms, biogenic opal, age model), PC (diatoms), AL (age model, diatoms), OE (diatom transfer function), GM (GDGTs, ^{14}C dating), AVH ($\delta^{13}$C IPSO[25]), NL ($\delta^{13}$C TOC), LLJ (foraminifera, age model), SMS (age model, humming age), JE, DE and CE provided temperature and salinity profiles near the study site. MV drafted the manuscript. All authors contributed to the interpretation and discussion of the data and the finalization of this manuscript.

**Competing interests**

None of the authors have a conflict of interest.

**Acknowledgement**

We thank the captain, crew and chief scientist Frank Lamy of RV Polarstern cruise PS97. Denise Diekstall, Jens Hefter, Alejandro Avila and Victor Acuña are thanked for their laboratory support. We thank Helge Arz for his help with the age model. Simon Belt is acknowledged for providing the 7-HND internal standard for HBI quantification. Financial support was provided through the Helmholtz Research grant VH-NG-1101. Partial support from the Centers IDEAL (grant FONDAP 15150003) and COPAS (grants AFB170006 and FB210021), Chile, and the Spanish Ministry of Economy, Industry and Competitivity grants CTM2017-89711-C2-½-P, co-funded by the European Union through FEDER funds, is acknowledged. We appreciate support by the Open Access Publication Funds of Alfred-Wegener-Institut Helmholtz-Zentrum für Polar- und Meeresforschung.

585 **References**

586 Alexander, V. and Niebauer, H. .: Oceanography of the eastern Bering Sea ice-edge zone in spring, Limn, 26(6),

587 1111–1125 [online] Available from: http://doi.wiley.com/10.1029/2007RG000250, 1981.

588 Allen, C. S., Oakes-Fretwell, L., Anderson, J. B. and Hodgson, D. A.: A record of Holocene glacial and

589 oceanographic variability in Neny Fjord, Antarctic Peninsula, The Holocene, 20(4), 551–564,

590 doi:10.1177/0959683609356581, 2010.

591 Allison, I., Tivendale, C. M., Akerman, G. J., Tann, J. M. and Wills, R. H.: Seasonal Variations In The Surface

592 Energy Exchanges Over Antarctic Sea Ice and Coastal Waters, Annals of Glaciology, 3, 12–16,

593 doi:10.3189/S0260305500002445, 1982.

594 Anderson, R. F., Ali, S., Bradtmiller, L. I., Nielsen, S. H. H., Fleisher, M. Q., Anderson, B. E. and Burckle, L.

595 H.: Wind-Driven Upwelling in the Southern Ocean and the Deglacial Rise in Atmospheric CO2, Science, 323,

596 1443–1448, doi:10.1126/science.1167441, 2009.

597 Armand, L. K. and Zielinski, U.: DIATOM SPECIES OF THE GENUS *RHIZOSOLENIA* FROM SOUTHERN

598 OCEAN SEDIMENTS: DISTRIBUTION AND TAXONOMIC NOTES, Diatom Research, 16(2), 259–294,

599 doi:10.1080/0269249X.2001.9705520, 2001.

600 Arrigo, K. R., Worthen, D. L., Lizotte, M. P., Dixon, P. and Dieckmann, G.: Primary Production in Antarctic Sea

601 Ice, Science, 276, 394–397, doi:10.1126/science.276.5311.394, 1997.

602 Barbara, L., Crosta, X., Schmidt, S. and Massé, G.: Diatoms and biomarkers evidence for major changes in sea

603 ice conditions prior the instrumental period in Antarctic Peninsula, Quaternary Science Reviews, 79, 99–110,

604 doi:10.1016/j.quascirev.2013.07.021, 2013.

605 Barbara, L., Crosta, X., Leventer, A., Schmidt, S., Etourneau, J., Domack, E. and Massé, G.: Environmental

606 responses of the Northeast Antarctic Peninsula to the Holocene climate variability, Paleoceanography, 31(1),

607 131–147, doi:10.1002/2015PA002785, 2016.

608 Bárcena, M. A., Gersonde, R., Ledesma, S., Fabrés, J., Calafat, A. M., Canals, M., Sierro, F. J. and Flores, J. A.:

609 Record of Holocene glacial oscillations in Bransfield Basin as revealed by siliceous microfossil assemblages,

610 Antarctic Science, 10(03), 269–285, doi:10.1017/S0954102098000364, 1998.

611 Belt, S. T.: Source-specific biomarkers as proxies for Arctic and Antarctic sea ice, Organic Geochemistry, 125,

612 277–298, doi:10.1016/j.orggeochem.2018.10.002, 2018.

613 Belt, S. T., Smik, L., Brown, T. A., Kim, J. H., Rowland, S. J., Allen, C. S., Gal, J. K., Shin, K. H., Lee, J. I. and

614 Taylor, K. W. R.: Source identification and distribution reveals the potential of the geochemical Antarctic sea ice

615 proxy IPSO25, Nature Communications, 7, 1–10, doi:10.1038/ncomms12655, 2016.

616 Belt, S. T. T., Brown, T. A. A., Ampel, L., Cabedo-Sanz, P., Fahl, K., Kocis, J. J. J., Massé, G., Navarro-

617 Rodriguez, A., Ruan, J. and Xu, Y.: An inter-laboratory investigation of the Arctic sea ice biomarker proxy IP25

618 in marine sediments: key outcomes and recommendations, Climate of the Past, 10(1), 155–166, doi:10.5194/cp-

619 10-155-2014, 2014.

620 Bentley, M. J., Hodgson, D. A., Smith, J. A., Cofaigh, C. ., Domack, E. W., Larter, R. D., Roberts, S. J.,

621 Brachfeld, S., Leventer, A., Hjort, C., Hillenbrand, C.-D. and Evans, J.: Mechanisms of Holocene

622 palaeoenvironmental change in the Antarctic Peninsula region, The Holocene, 19(1), 51–69,

623 doi:10.1177/0959683608096603, 2009.

624 Bentley, M. J., Ó Cofaigh, C., Anderson, J. B., Conway, H., Davies, B., Graham, A. G. C., Hillenbrand, C.-D.,

625 Hodgson, D. A., Jamieson, S. S. R., Larter, R. D., Mackintosh, A., Smith, J. A., Verleyen, E., Ackert, R. P., Bart,

626 P. J., Berg, S., Brunstein, D., Canals, M., Colhoun, E. A., Crosta, X., Dickens, W. A., Domack, E., Dowdeswell,

627 J. A., Dunbar, R., Ehrmann, W., Evans, J., Favier, V., Fink, D., Fogwill, C. J., Glasser, N. F., Gohl, K.,

628 Golledge, N. R., Goodwin, I., Gore, D. B., Greenwood, S. L., Hall, B. L., Hall, K., Hedding, D. W., Hein, A. S.,

629 Hocking, E. P., Jakobsson, M., Johnson, J. S., Jomelli, V., Jones, R. S., Klages, J. P., Kristoffersen, Y., Kuhn,

630 G., Leventer, A., Licht, K., Lilly, K., Lindow, J., Livingstone, S. J., Massé, G., McGlone, M. S., McKay, R. M.,

631 Melles, M., Miura, H., Mulvaney, R., Nel, W., Nitsche, F. O., O'Brien, P. E., Post, A. L., Roberts, S. J.,

632 Saunders, K. M., Selkirk, P. M., Simms, A. R., Spiegel, C., Stolldorf, T. D., Sugden, D. E., van der Putten, N.,

633 van Ommen, T., Verfaillie, D., Vyverman, W., Wagner, B., White, D. A., Witus, A. E. and Zwartz, D.: A

634 community-based geological reconstruction of Antarctic Ice Sheet deglaciation since the Last Glacial Maximum,

635 Quaternary Science Reviews, 100(August), 1–9, doi:10.1016/j.quascirev.2014.06.025, 2014.

636 Blunier, T. and Brook, E. J.: Timing of millennial-scale climate change in antarctica and greenland during the

637 last glacial period, Science, 291(5501), 109–112, doi:10.1126/science.291.5501.109, 2001.

638 Boyer, T., Garcia, H. E., Locarnini, R. A., Zweng, M. M., Mishonov, A. V and Reagan, J. R.: Wolrd Ocean

639 Atlas 2018., 2018.

640 Bracegirdle, T. J., Stephenson, D. B., Turner, J. and Phillips, T.: The importance of sea ice area biases in 21st

641 century multimodel projections of Antarctic temperature and precipitation, Geophysical Research Letters,

642 42(24), 10,832-10,839, doi:10.1002/2015GL067055, 2015.

643 Bracegirdle, T. J., Colleoni, F., Abram, N. J., Bertler, N. A. N., Dixon, D. A., England, M., Favier, V., Fogwill,

644 C. J., Fyfe, J. C., Goodwin, I., Goosse, H., Hobbs, W., Jones, J. M., Keller, E. D., Khan, A. L., Phipps, S. J.,

645 Raphael, M. N., Russell, J., Sime, L., Thomas, E. R., van den Broeke, M. R. and Wainer, I.: Back to the Future:

646 Using Long-Term Observational and Paleo-Proxy Reconstructions to Improve Model Projections of Antarctic

647 Climate, Geosciences, 9(6), 255, doi:10.3390/geosciences9060255, 2019.

648 Broecker, W. S.: Paleocean circulation during the Last Deglaciation: A bipolar seesaw?, Paleoceanography,

649 13(2), 119–121, doi:10.1029/97PA03707, 1998.

650 Buffen, A., Leventer, A., Rubin, A. and Hutchins, T.: Diatom assemblages in surface sediments of the

651 northwestern Weddell Sea, Antarctic Peninsula, Marine Micropaleontology, 62(1), 7–30,

652 doi:10.1016/J.MARMICRO.2006.07.002, 2007.

653 Butterworth, B. J. and Miller, S. D.: Air-sea exchange of carbon dioxide in the Southern Ocean and Antarctic

654 marginal ice zone, Geophysical Research Letters, 43(13), 7223–7230, doi:10.1002/2016GL069581, 2016.

655 Butzin, M., Köhler, P. and Lohmann, G.: Marine radiocarbon reservoir age simulations for the past 50,000 years,

656 Geophysical Research Letters, 44(16), 8473–8480, doi:10.1002/2017GL074688, 2017.

657 Cádiz Hernández, A.: Evidencia de cambios en la productividad marina a partir de testigos sedimentarios

658 recuperados en Bahía Fildes (Maxwell Bay) y Costa de Palmer, Península Antártica durante los últimos ~ 1000

659 años, Universidad de Valparaíso., 2019.

660 Canals, M. and Amblas, D.: Seafloor kettle holes in Orleans Trough, Bransfield Basin, Antarctic Peninsula,

661 Geological Society, London, Memoirs, 46(1), 313–314, doi:10.1144/M46.16, 2016a.

662 Canals, M. and Amblas, D.: The bundle: a mega-scale glacial landform left by an ice stream, Western Bransfield

663 Basin, Geological Society, London, Memoirs, 46(1), 177–178, doi:10.1144/M46.157, 2016b.

664 Canals, M., Amblas, D. and Casamor, J. L.: Cross-shelf troughs in Central Bransfield Basin, Antarctic Peninsula,

665 Geological Society, London, Memoirs, 46(1), 171–172, doi:10.1144/M46.138, 2016.

666 Cárdenas, P., Lange, C. B., Vernet, M., Esper, O., Srain, B., Vorrath, M.-E. M.-E., Ehrhardt, S., Müller, J.,

667 Kuhn, G., Arz, H. W. H. W. H. W., Lembke-Jene, L., Lamy, F. and Paola Cárdenas, Carina B. Lange, Maria

668 Vernet, Oliver Esper, Benjamin Srain, Maria-Elena Vorrath, Sophie Ehrhardt, Juliane Müller, Gerhard Kuhn,

669 Helge W.Arz, Lester Lembke-Jene, F. L.: Biogeochemical proxies and diatoms in surface sediments across the

670 Drake Passage reflect oceanic domains and frontal systems in the region, Progress in Oceanography, 174, 72–88,

671 doi:10.1016/j.pocean.2018.10.004, 2019.

672 Carrasco, J. F., Bozkurt, D. and Cordero, R. R.: A review of the observed air temperature in the Antarctic

673 Peninsula. Did the warming trend come back after the early 21st hiatus?, Polar Science, 28, 100653,

674 doi:10.1016/j.polar.2021.100653, 2021.

675 Cavalieri, D. J., Parkinson, C. L., Gloersen, P. and Zwally, H. J.: Sea Ice Concentrations from Nimbus-7 SMMR

676 and DMSP SSM/I-SSMIS Passive Microwave Data, Version 1, Boulder, Colorado USA,

677 doi:10.5067/8GQ8LZQVL0VL, 1996.

678     Chisholm, S. W.: Stirring times in the Southern Ocean, Nature, 407(6805), 685–686, doi:10.1038/35037696,

679     2000.

680     Clark, P. U., Shakun, J. D., Baker, P. A., Bartlein, P. J., Brewer, S., Brook, E., Carlson, A. E., Cheng, H.,

681     Kaufman, D. S., Liu, Z., Marchitto, T. M., Mix, A. C., Morrill, C., Otto-Bliesner, B. L., Pahnke, K., Russell, J.

682     M., Whitlock, C., Adkins, J. F., Blois, J. L., Clark, J., Colman, S. M., Curry, W. B., Flower, B. P., He, F.,

683     Johnson, T. C., Lynch-Stieglitz, J., Markgraf, V., McManus, J., Mitrovica, J. X., Moreno, P. I. and Williams, J.

684     W.: Global climate evolution during the last deglaciation, Proceedings of the National Academy of Sciences,

685     109(19), E1134–E1142, doi:10.1073/pnas.1116619109, 2012.

686     Collares, L. L., Mata, M. M., Kerr, R., Arigony-Neto, J. and Barbat, M. M.: Iceberg drift and ocean circulation

687     in the northwestern Weddell Sea, Antarctica, Deep Sea Research Part II: Topical Studies in Oceanography,

688     149(January 2019), 10–24, doi:10.1016/j.dsr2.2018.02.014, 2018.

689     Cook, A. J., Holland, P. R., Meredith, M. P., Murray, T., Luckman, A. and Vaughan, D. G.: Ocean forcing of

690     glacier retreat in the western Antarctic Peninsula, Science, 353(6296), 283–286, doi:10.1126/science.aae0017,

691     2016.

692     Couto, N., Martinson, D. G., Kohut, J. and Schofield, O.: Distribution of Upper Circumpolar Deep Water on the

693     warming continental shelf of the West Antarctic Peninsula, Journal of Geophysical Research: Oceans, 122(7),

694     5306–5315, doi:10.1002/2017JC012840, 2017.

695     Crosta, X., Kohfeld, K. E., Bostock, H. C., Chadwick, M., Du Vivier, A., Esper, O., Etourneau, J., Jones, J.,

696     Leventer, A., Müller, J., Rhodes, R. H., Allen, C. S., Ghadi, P., Lamping, N., Lange, C. B., Lawler, K.-A., Lund,

697     D., Marzocchi, A., Meissner, K. J., Menviel, L., Nair, A., Patterson, M., Pike, J., Prebble, J. G., Riesselman, C.,

698     Sadatzki, H., Sime, L. C., Shukla, S. K., Thöle, L., Vorrath, M.-E., Xiao, W. and Yang, J.: Antarctic sea ice over

699     the past 130,000 years, Part 1: A review of what proxy records tell us, EGUsphere [preprint],

700     doi:10.5194/egusphere-2022-99, 2022.

701     Denis, D., Crosta, X., Barbara, L., Massé, G., Renssen, H., Ther, O. and Giraudeau, J.: Sea ice and wind

702     variability during the Holocene in East Antarctica: insight on middle–high latitude coupling, Quaternary Science

703     Reviews, 29(27–28), 3709–3719, doi:10.1016/J.QUASCIREV.2010.08.007, 2010.

704     Domack, E., Leventer, A., Dunbar, R., Taylor, F., Brachfeld, S. and Sjunneskogs, C.: Chronology of the Palmer

705     Deep site, Antarctic Peninsula: a Holocene palaeoenvironmental reference for the circum-Antarctic, The

706     Holocene, 11(1), 1–9, doi:10.1191/095968301673881493, 2001.

707     Domack, E. W.: A Synthesis for Site 1098: Palmer Deep, in Proceedings of the Ocean Drilling Program, 178

708     Scientific Results, Ocean Drilling Program., 2002.

709     Ducklow, H. W., Erickson, M., Kelly, J., Montes-Hugo, M., Ribic, C. A., Smith, R. C., Stammerjohn, S. E. and

710     Karl, D. M.: Particle export from the upper ocean over the continental shelf of the west Antarctic Peninsula: A

711     long-term record, 1992–2007, Deep Sea Research Part II: Topical Studies in Oceanography, 55(18–19), 2118–

712     2131, doi:10.1016/j.dsr2.2008.04.028, 2008.

713     EPICA Community Members: Eight glacial cycles from an Antarctic ice core, Nature, 429(6992), 623–628,

714     doi:10.1038/nature02599, 2004.

715     EPICA Community Members: One-to-one coupling of glacial climate variability in Greenland and Antarctica,

716     Nature, 444(7116), 195–198, doi:10.1038/nature05301, 2006.

717     Escutia, C., DeConto, R., Dunbar, R., De Santis, L., Shevenell, A. and Nash, T.: Keeping an Eye on Antarctic

718     Ice Sheet Stability, Oceanography, 32(1), 32–46, doi:10.5670/oceanog.2019.117, 2019.

719     Esper, O. and Gersonde, R.: New tools for the reconstruction of Pleistocene Antarctic sea ice, Palaeogeography,

720     Palaeoclimatology, Palaeoecology, 399, 260–283, doi:10.1016/J.PALAEO.2014.01.019, 2014a.

721     Esper, O. and Gersonde, R.: Quaternary surface water temperature estimations: New diatom transfer functions

722     for the Southern Ocean, Palaeogeography, Palaeoclimatology, Palaeoecology, 414, 1–19,

723     doi:10.1016/J.PALAEO.2014.08.008, 2014b.

724     Esper, O., Gersonde, R. and Kadagies, N.: Diatom distribution in southeastern Pacific surface sediments and

725     their relationship to modern environmental variables, Palaeogeography, Palaeoclimatology, Palaeoecology,

726     287(1–4), 1–27, doi:10.1016/J.PALAEO.2009.12.006, 2010.

727     Etourneau, J., Collins, L. G., Willmott, V., Kim, J. H., Barbara, L., Leventer, A., Schouten, S., Sinninghe

728     Damsté, J. S., Bianchini, A., Klein, V., Crosta, X. and Massé, G.: Holocene climate variations in the western

729     Antarctic Peninsula: Evidence for sea ice extent predominantly controlled by changes in insolation and ENSO

730     variability, Climate of the Past, 9(4), 1431–1446, doi:10.5194/cp-9-1431-2013, 2013.

731     Etourneau, J., Sgubin, G., Crosta, X., Swingedouw, D., Willmott, V., Barbara, L., Houssais, M. N., Schouten, S.,

732     Damsté, J. S. S., Goosse, H., Escutia, C., Crespin, J., Massé, G. and Kim, J. H.: Ocean temperature impact on ice

733     shelf extent in the eastern Antarctic Peninsula, Nature Communications, 10(1), 8–15, doi:10.1038/s41467-018-

734     08195-6, 2019.

735     Fietz, S., Huguet, C., Rueda, G., Hambach, B. and Rosell-Melé, A.: Hydroxylated isoprenoidal GDGTs in the

736     Nordic Seas, Marine Chemistry, 152, 1–10, doi:10.1016/j.marchem.2013.02.007, 2013.

737     Fischer, H., Fundel, F., Ruth, U., Twarloh, B., Wegner, A., Udisti, R., Becagli, S., Castellano, E., Morganti, A.,

738     Severi, M., Wolff, E., Littot, G., Röthlisberger, R., Mulvaney, R., Hutterli, M. A., Kaufmann, P., Federer, U.,

739     Lambert, F., Bigler, M., Hansson, M., Jonsell, U., de Angelis, M., Boutron, C., Siggaard-Andersen, M.-L.,

740    Steffensen, J. P., Barbante, C., Gaspari, V., Gabrielli, P. and Wagenbach, D.: Reconstruction of millennial

741    changes in dust emission, transport and regional sea ice coverage using the deep EPICA ice cores from the

742    Atlantic and Indian Ocean sector of Antarctica, Earth and Planetary Science Letters, 260(1–2), 340–354,

743    doi:10.1016/j.epsl.2007.06.014, 2007.

744    Fletcher, M.-S., Pedro, J., Hall, T., Mariani, M., Alexander, J. A., Beck, K., Blaauw, M., Hodgson, D. A.,

745    Heijnis, H., Gadd, P. S. and Lise-Pronovost, A.: Northward shift of the southern westerlies during the Antarctic

746    Cold Reversal, Quaternary Science Reviews, 271, 107189, doi:10.1016/j.quascirev.2021.107189, 2021.

747    Gersonde, R. and Zielinski, U.: The reconstruction of late Quaternary Antarctic sea-ice distribution — the use of

748    diatoms as a proxy for sea-ice, , 162, 263–286, doi:10.1016/S0031-0182(00)00131-0, 2000.

749    Gersonde, R., Crosta, X., Abelmann, A. and Armand, L.: Sea-surface temperature and sea ice distribution of the

750    Southern Ocean at the EPILOG Last Glacial Maximum—a circum-Antarctic view based on siliceous microfossil

751    records, Quaternary Science Reviews, 24(7–9), 869–896, doi:10.1016/J.QUASCIREV.2004.07.015, 2005.

752    Gloersen, P., Campbell, W. J., Cavalieri, D. J., Comiso, J. C., Parkinson, C. L. and Zwally, H. J.: Arctic and

753    antarctic sea ice, 1978, Annals of Glaciology, 17, 149–154, 1993.

754    Gonçalves-Araujo, R., de Souza, M. S., Tavano, V. M. and Garcia, C. A. E.: Influence of oceanographic features

755    on spatial and interannual variability of phytoplankton in the Bransfield Strait, Antarctica, Journal of Marine

756    Systems, 142, 1–15, doi:10.1016/J.JMARSYS.2014.09.007, 2015.

757    Han, Z., Hu, C., Sun, W., Zhao, J., Pan, J., Fan, G. and Zhang, H.: Characteristics of particle fluxes in the Prydz

758    Bay polynya, Eastern Antarctica, Science China Earth Sciences, 62(4), 657–670, doi:10.1007/s11430-018-9285-

759    6, 2019.

760    Hellmer, H. H., Kauker, F., Timmermann, R., Determann, J. and Rae, J.: Twenty-first-century warming of a

761    large Antarctic ice-shelf cavity by a redirected coastal current, Nature, 485(7397), 225–228,

762    doi:10.1038/nature11064, 2012.

763    Heroy, D. C., Sjunneskog, C. and Anderson, J. B.: Holocene climate change in the Bransfield Basin, Antarctic

764    Peninsula: evidence from sediment and diatom analysis, Antarctic Science, 20(01), 69–87,

765    doi:10.1017/S0954102007000788, 2008.

766    Hillaire-Marcel, C. and de Vernal, A.: Proxies in Late Cenozoic Paleoceanography, edited by C. Hillaire-Marcel

767    and A. de Vernal, Elsevier, Amsterdam., 2007.

768    Hofmann, E. E., Klinck, J. M., Lascara, C. M. and Smith, D. A.: Water mass distribution and circulation west of

769    the Antarctic Peninsula and including Bransfield Strait, pp. 61–80, American Geophysical Union (AGU)., 1996.

770    Hopmans, E. C., Weijers, J. W. H., Schefuß, E., Herfort, L., Sinninghe Damsté, J. S. and Schouten, S.:

771 Variability in the Benguela Current upwelling system over the past 70,000 years, Earth and Planetary Science

772 Letters, 224(1–2), 107–116, doi:10.1016/j.epsl.2004.05.012, 2004.

773 Huss, M. and Farinotti, D.: A high-resolution bedrock map for the Antarctic Peninsula, The Cryosphere, 8(4),

774 1261–1273, doi:10.5194/tc-8-1261-2014, 2014.

775 Ingólfsson, Ó., Hjort, C. and Humlum, O.: Glacial and Climate History of the Antarctic Peninsula since the Last

776 Glacial Maximum, Arctic, Antarctic, and Alpine Research, 35(2), 175–186, doi:10.1657/1523-

777 0430(2003)035[0175:GACHOT]2.0.CO;2, 2003.

778 IPCC: Summary for Policymakers, in Climate Change 2021_ The Physical Science Basis. Contribution of

779 working Group I to the Sixth Assessment Report of the Intergovernmental Panel on Climate Change, edited by

780 V. Masson-Delmotte, P. Zhai, H.-O. Pörtner, D. Roberts, J. Skea, P. R. Shukla, A. Pirani, W. Moufouma-Okia,

781 C. Péan, R. Pidcock, S. Connors, J. B. R. Matthews, Y. Chen, X. Zhou, M. I. Gomis, E. Lonnoy, T. Maycock,

782 M. Tignor, and T. Waterfield, p. 32, Cambridge University Press., 2021.

783 Jones, R. S., Johnson, J. S., Lin, Y., Mackintosh, A. N., Sefton, J. P., Smith, J. A., Thomas, E. R. and

784 Whitehouse, P. L.: Stability of the Antarctic Ice Sheet during the pre-industrial Holocene, Nature Reviews Earth

785 & Environment, 3(8), 500–515, doi:10.1038/s43017-022-00309-5, 2022.

786 Jouzel, J., Vaikmae, R., Petit, J. R., Martin, M., Duclos, Y., Stievenard, M., Lorius, C., Toots, M., Mélières, M.

787 A., Burckle, L. H., Barkov, N. I. and Kotlyakov, V. M.: The two-step shape and timing of the last deglaciation in

788 Antarctica, Climate Dynamics, 11(3), 151–161, doi:10.1007/BF00223498, 1995.

789 Kalanetra, K. M., Bano, N. and Hollibaugh, J. T.: Ammonia-oxidizing Archaea in the Arctic Ocean and

790 Antarctic coastal waters, Environmental Microbiology, 11(9), 2434–2445, doi:10.1111/j.1462-

791 2920.2009.01974.x, 2009.

792 Kim, D., Kim, D. Y., Kim, Y. J., Kang, Y. C. and Shim, J.: Downward fluxes of biogenic material in Bransfield

793 Strait, Antarctica, Antarctic Science, 16(3), 227–237, doi:10.1017/S0954102004002032, 2004.

794 Kim, J.-H., van der Meer, J., Schouten, S., Helmke, P., Willmott, V., Sangiorgi, F., Koç, N., Hopmans, E. C. and

795 Damsté, J. S. S.: New indices and calibrations derived from the distribution of crenarchaeal isoprenoid tetraether

796 lipids: Implications for past sea surface temperature reconstructions, Geochimica et Cosmochimica Acta, 74(16),

797 4639–4654, doi:10.1016/j.gca.2010.05.027, 2010.

798 Kim, J.-H., Crosta, X., Willmott, V., Renssen, H., Bonnin, J., Helmke, P., Schouten, S. and Sinninghe Damsté, J.

799 S.: Holocene subsurface temperature variability in the eastern Antarctic continental margin, Geophysical

800 Research Letters, 39(6), doi:10.1029/2012GL051157, 2012.

801 Klunder, M. B., Laan, P., De Baar, H. J. W., Middag, R., Neven, I. and Van Ooijen, J.: Dissolved Fe across the

802    Weddell Sea and Drake Passage: impact of DFe on nutrient uptake, Biogeosciences, 11(3), 651–669,

803    doi:10.5194/bg-11-651-2014, 2014.

804    Kyrmanidou, A., Vadman, K. J., Ishman, S. E., Leventer, A., Brachfeld, S., Domack, E. W. and Wellner, J. S.:

805    Late Holocene oceanographic and climatic variability recorded by the Perseverance Drift, northwestern Weddell

806    Sea, based on benthic foraminifera and diatoms, Marine Micropaleontology, 141, 10–22,

807    doi:10.1016/j.marmicro.2018.03.001, 2018.

808    Lamping, N., Müller, J., Esper, O., Hillenbrand, C., Smith, J. A. and Kuhn, G.: Highly branched isoprenoids

809    reveal onset of deglaciation followed by dynamic sea-ice conditions in the western Amundsen Sea, Antarctica,

810    Quaternary Science Reviews, 228, 106103, doi:10.1016/j.quascirev.2019.106103, 2020.

811    Lamping, N., Müller, J., Hefter, J., Mollenhauer, G., Haas, C., Shi, X., Vorrath, M.-E., Lohmann, G. and

812    Hillenbrand, C.-D.: Evaluation of lipid biomarkers as proxies for sea ice and ocean temperatures along the

813    Antarctic continental margin, Climate of the Past, 17(5), 2305–2326, doi:10.5194/cp-17-2305-2021, 2021.

814    Lamy, F.: The expedition PS97 of the research vessel POLARSTERN to the Drake Passage in 2016, Reports on

815    Polar and Marine Research, 7'01, 1–571, doi:10.2312/BzPM_0702_2016, 2016.

816    Lamy, F., Kaiser, J., Arz, H. W., Hebbeln, D., Ninnemann, U., Timm, O., Timmermann, A. and Toggweiler, J.

817    R.: Modulation of the bipolar seesaw in the Southeast Pacific during Termination 1, Earth and Planetary Science

818    Letters, 259(3–4), 400–413, doi:10.1016/j.epsl.2007.04.040, 2007.

819    Liu, R., Han, Z., Zhao, J., Zhang, H., Li, D., Ren, J., Pan, J. and Zhang, H.: Distribution and source of glycerol

820    dialkyl glycerol tetraethers (GDGTs) and the applicability of GDGT-based temperature proxies in surface

821    sediments of Prydz Bay, East Antarctica, Polar Research, 39, doi:10.33265/polar.v39.3557, 2020.

822    Locarnini, M., Mishonov, A., Baranova, O., Boyer, T., Zweng, M., Garcia, H., Reagan, J., Seidov, D., Weathers,

823    K., Paver, C. and Smolyar, I.: World Ocean Atlas 2018, Volume 1: Temperature. [online] Available from:

824    https://archimer.ifremer.fr/doc/00651/76338/, 2018.

825    Lü, X., Liu, X. L., Elling, F. J., Yang, H., Xie, S., Song, J., Li, X., Yuan, H., Li, N. and Hinrichs, K. U.:

826    Hydroxylated isoprenoid GDGTs in Chinese coastal seas and their potential as a paleotemperature proxy for

827    mid-to-low latitude marginal seas, Organic Geochemistry, 89–90, 31–43,

828    doi:10.1016/j.orggeochem.2015.10.004, 2015.

829    Martinson, D. G. and McKee, D. C.: Transport of warm Upper Circumpolar Deep Water onto the western

830    Antarctic Peninsula continental shelf, Ocean Science, 8(4), 433–442, doi:10.5194/os-8-433-2012, 2012.

831    Massé, G., Belt, S. T., Crosta, X., Schmidt, S., Snape, I., Thomas, D. N. and Rowland, S. J.: Highly branched

832    isoprenoids as proxies for variable sea ice conditions in the Southern Ocean, Antarctic Science, 23(05), 487–498,

doi:10.1017/S0954102011000381, 2011.

McClymont, E. L., Bentley, M. J., Hodgson, D. A., Spencer-Jones, C. L., Wardley, T., West, M. D., Croudace, I. W., Berg, S., Gröcke, D. R., Kuhn, G., Jamieson, S. S. R., Sime, L. and Phillips, R. A.: Summer sea-ice variability on the Antarctic margin during the last glacial period reconstructed from snow petrel (Pagodroma nivea) stomach-oil deposits, Climate of the Past, 18(2), 381–403, doi:10.5194/cp-18-381-2022, 2022.

Meredith, M. P. and King, J. C.: Rapid climate change in the ocean west of the Antarctic Peninsula during the second half of the 20th century, Geophysical Research Letters, 32(19), 1–5, doi:10.1029/2005GL024042, 2005.

Milliken, K. T., Anderson, J. B., Wellner, J. S., Bohaty, S. M. and Manley, P. L.: High-resolution Holocene climate record from Maxwell Bay, South Shetland Islands, Antarctica, Geological Society of America Bulletin, 121(11–12), 1711–1725, doi:10.1130/B26478.1, 2009.

Minzoni, R. T., Anderson, J. B., Fernandez, R. and Wellner, J. S.: Marine record of Holocene climate, ocean, and cryosphere interactions: Herbert Sound, James Ross Island, Antarctica, Quaternary Science Reviews, 129, 239–259, doi:10.1016/j.quascirev.2015.09.009, 2015.

Mollenhauer, G., Grotheer, H., Gentz, T., Bonk, E. and Hefter, J.: Standard operation procedures and performance of the MICADAS radiocarbon laboratory at Alfred Wegener Institute (AWI), Germany, Nuclear Instruments and Methods in Physics Research Section B: Beam Interactions with Materials and Atoms, 496, 45–51, doi:10.1016/j.nimb.2021.03.016, 2021.

Morigi, C., Capotondi, L., Giglio, F., Langone, L., Brilli, M., Turi, B. and Ravaioli, M.: A possible record of the Younger Dryas event in deep-sea sediments of the Southern Ocean (Pacific sector), in Palaeogeography, Palaeoclimatology, Palaeoecology, vol. 198, pp. 265–278, Elsevier B.V., 2003.

Mortlock, R. A. and Froelich, P. N.: A simple method for the rapid determination of biogenic opal in pelagic marine sediments, Deep Sea Research Part A, Oceanographic Research Papers, 36(9), 1415–1426, doi:10.1016/0198-0149(89)90092-7, 1989.

Müller, J., Wagner, A., Fahl, K., Stein, R., Prange, M. and Lohmann, G.: Towards quantitative sea ice reconstructions in the northern North Atlantic: A combined biomarker and numerical modelling approach, Earth and Planetary Science Letters, 306(3–4), 137–148, doi:10.1016/J.EPSL.2011.04.011, 2011.

Müller, P. J. and Schneider, R.: An automated leaching method for the determination of opal in sediments and particulate matter, Deep-Sea Research Part I, 40(3), 425–444, doi:https://doi.org/10.1016/0967-0637(93)90140-X, 1993.

Mulvaney, R., Abram, N. J., Hindmarsh, R. C. A., Arrowsmith, C., Fleet, L., Triest, J., Sime, L. C., Alemany, O. and Foord, S.: Recent Antarctic Peninsula warming relative to Holocene climate and ice-shelf history, Nature,

864    489(7414), 141–144, doi:10.1038/nature11391, 2012.

865    Murray, A. E., Preston, C. M., Massana, R., Taylor, L. T., Blakis, A., Wu, K. and DeLong, E. F.: Seasonal and

866    Spatial Variability of Bacterial and Archaeal Assemblages in the Coastal Waters near Anvers Island, Antarctica,

867    Applied and Environmental Microbiology, 64(7), 2585–2595, doi:10.1128/AEM.64.7.2585-2595.1998, 1998.

868    Nicholls, K. W., Østerhus, S., Makinson, K., Gammelsrød, T. and Fahrbach, E.: Ice-ocean processes over the

869    continental shelf of the southern Weddell Sea, Antarctica: A review, Reviews of Geophysics, 47(3), RG3003,

870    doi:10.1029/2007RG000250, 2009.

871    Ó Cofaigh, C., Davies, B. J., Livingstone, S. J., Smith, J. A., Johnson, J. S., Hocking, E. P., Hodgson, D. A.,

872    Anderson, J. B., Bentley, M. J., Canals, M., Domack, E., Dowdeswell, J. A., Evans, J., Glasser, N. F.,

873    Hillenbrand, C.-D., Larter, R. D., Roberts, S. J. and Simms, A. R.: Reconstruction of ice-sheet changes in the

874    Antarctic Peninsula since the Last Glacial Maximum, Quaternary Science Reviews, 100, 87–110,

875    doi:10.1016/j.quascirev.2014.06.023, 2014.

876    Oksanen, J., Blanchet, F. G., Kindt, R., Legendre, P., Minchin, P. R., O´Hara, R. B., Simpson, G. L., Solymos,

877    P., Stevens, M. H. H. and Wagner, H.: Vegan: Community Ecology Package (R Package Version 2.0-3), 2012.

878    Parkinson, C. L. and Cavalieri, D. J.: Antarctic sea ice variability and trends, 1979–2010, The Cryosphere, 6,

879    871–880, doi:10.5194/tc-6-871-2012, 2012.

880    Pedro, J. B., Bostock, H. C., Bitz, C. M., He, F., Vandergoes, M. J., Steig, E. J., Chase, B. M., Krause, C. E.,

881    Rasmussen, S. O., Markle, B. R. and Cortese, G.: The spatial extent and dynamics of the Antarctic Cold

882    Reversal, Nature Geoscience, 9(1), 51–55, doi:10.1038/ngeo2580, 2016.

883    QGIS, D. T.: QGIS Geographic Information System, [online] Available from: http://qgis.osgeo.org, 2018.

884    R Core Team: R: a Language and Environment for Statistical Computing, R Foundation for Statistical

885    computing, Vienna., 2012.

886    Reimer, P. J., Austin, W. E. N., Bard, E., Bayliss, A., Blackwell, P. G., Bronk Ramsey, C., Butzin, M., Cheng,

887    H., Edwards, R. L., Friedrich, M., Grootes, P. M., Guilderson, T. P., Hajdas, I., Heaton, T. J., Hogg, A. G.,

888    Hughen, K. A., Kromer, B., Manning, S. W., Muscheler, R., Palmer, J. G., Pearson, C., van der Plicht, J.,

889    Reimer, R. W., Richards, D. A., Scott, E. M., Southon, J. R., Turney, C. S. M., Wacker, L., Adolphi, F.,

890    Büntgen, U., Capano, M., Fahrni, S. M., Fogtmann-Schulz, A., Friedrich, R., Köhler, P., Kudsk, S., Miyake, F.,

891    Olsen, J., Reinig, F., Sakamoto, M., Sookdeo, A. and Talamo, S.: The IntCal20 Northern Hemisphere

892    Radiocarbon Age Calibration Curve (0–55 cal kBP), Radiocarbon, 62(4), 725–757, doi:10.1017/RDC.2020.41,

893    2020.

894    Reynolds, R. W., Rayner, N. A., Smith, T. M., Stokes, D. C., Wang, W., Reynolds, R. W., Rayner, N. A., Smith,

895    T. M., Stokes, D. C. and Wang, W.: An Improved In Situ and Satellite SST Analysis for Climate, Journal of

896    Climate, 15(13), 1609–1625, doi:10.1175/1520-0442(2002)015<1609:AIISAS>2.0.CO;2, 2002.

897    Reynolds, R. W., Smith, T. M., Liu, C., Chelton, D. B., Casey, K. S., Schlax, M. G., Reynolds, R. W., Smith, T.

898    M., Liu, C., Chelton, D. B., Casey, K. S. and Schlax, M. G.: Daily High-Resolution-Blended Analyses for Sea

899    Surface Temperature, Journal of Climate, 20(22), 5473–5496, doi:10.1175/2007JCLI1824.1, 2007.

900    Rignot, E., Mouginot, J., Scheuchl, B., van den Broeke, M., van Wessem, M. J. and Morlighem, M.: Four

901    decades of Antarctic Ice Sheet mass balance from 1979–2017, Proceedings of the National Academy of

902    Sciences, 116(4), 1095–1103, doi:10.1073/pnas.1812883116, 2019.

903    Roche, D. M., Crosta, X. and Renssen, H.: Evaluating Southern Ocean sea-ice for the Last Glacial Maximum

904    and pre-industrial climates: PMIP-2 models and data evidence, Quaternary Science Reviews, 56, 99–106,

905    doi:10.1016/j.quascirev.2012.09.020, 2012.

906    Ronge, T. A., Lippold, J., Geibert, W., Jaccard, S. L., Mieruch-Schnülle, S., Süfke, F. and Tiedemann, R.:

907    Deglacial patterns of South Pacific overturning inferred from 231Pa and 230Th, Scientific Reports, 11(1),

908    doi:10.1038/s41598-021-00111-1, 2021.

909    Roseby, Z. A., Smith, J. A., Hillenbrand, C.-D., Cartigny, M. J. B., Rosenheim, B. E., Hogan, K. A., Allen, C.

910    S., Leventer, A., Kuhn, G., Ehrmann, W. and Larter, R. D.: History of Anvers-Hugo Trough, western Antarctic

911    Peninsula shelf, since the Last Glacial Maximum. Part I: Deglacial history based on new sedimentological and

912    chronological data, Quaternary Science Reviews, 291, 107590, doi:10.1016/j.quascirev.2022.107590, 2022.

913    Ruiz Barlett, E. M., Tosonotto, G. V., Piola, A. R., Sierra, M. E. and Mata, M. M.: On the temporal variability of

914    intermediate and deep waters in the Western Basin of the Bransfield Strait, Deep Sea Research Part II: Topical

915    Studies in Oceanography, 149, 31–46, doi:10.1016/j.dsr2.2017.12.010, 2018.

916    Sangrà, P., Gordo, C., Hernández-Arencibia, M., Marrero-Díaz, A., Rodríguez-Santana, A., Stegner, A.,

917    Martínez-Marrero, A., Pelegrí, J. L. and Pichon, T.: The Bransfield current system, Deep Sea Research Part I:

918    Oceanographic Research Papers, 58(4), 390–402, doi:10.1016/J.DSR.2011.01.011, 2011.

919    Sangrà, P., Stegner, A., Hernández-Arencibia, M., Marrero-Díaz, Á., Salinas, C., Aguiar-González, B.,

920    Henríquez-Pastene, C. and Mouriño-Carballido, B.: The Bransfield Gravity Current, Deep-Sea Research Part I:

921    Oceanographic Research Papers, 119(November 2016), 1–15, doi:10.1016/j.dsr.2016.11.003, 2017.

922    Scherer, R. P.: A new method for the determination of absolute abundance of diatoms and other silt-sized

923    sedimentary particles, Journal of Paleolimnology, 12(2), 171–179, doi:10.1007/BF00678093, 1994.

924    Schlüter, M. and Rickert, D.: Effect of pH on the measurement of biogenic silica, Marine Chemistry, 63(1–2),

925    81–92, doi:10.1016/S0304-4203(98)00052-8, 1998.

926    Schofield, O., Brown, M., Kohut, J., Nardelli, S., Saba, G., Waite, N. and Ducklow, H.: Changes in the upper

927    ocean mixed layer and phytoplankton productivity along the West Antarctic Peninsula, Philosophical

928    Transactions of the Royal Society A: Mathematical, Physical and Engineering Sciences, 376(2122),

929    doi:10.1098/rsta.2017.0173, 2018.

930    Schrader, H. and Gersonde, R.: Diatoms and silicoflagellates, in Micropaleontological Methods and Techniques

931    - An Excercise on an Eight Meter Section of the Lower Pliocene of Capo Rossello, Sicily, Utrecht

932    Micropaleontological Bulletins, vol. 17, edited by W. J. Zachariasse, W. R. Riedel, A. Sanfilippo, R. R. Schmidt,

933    M. J. Brolsma, H. J. Schrader, R. Gersonde, M. M. Drooger, and J. A. Broekman, pp. 129–176., 1978.

934    Shevenell, A. E., Ingalls, A. E., Domack, E. W. and Kelly, C.: Holocene Southern Ocean surface temperature

935    variability west of the Antarctic Peninsula, Nature, 470(7333), 250–254, doi:10.1038/nature09751, 2011.

936    Simpson, G. L. and Oksanen, J.: Analogue: Analogue Matching and Modern Analogue Technique Transfer

937    Function Models. R Package Version 0.8-2, 2012.

938    Sjunneskog, C. and Taylor, F.: Postglacial marine diatom record of the Palmer Deep, Antarctic Peninsula (ODP

939    Leg 178, Site 1098) 1. Total diatom abundance, Paleoceanography, 17(3), PAL 4-1-PAL 4-8,

940    doi:10.1029/2000PA000563, 2002.

941    Stenni, B., Masson-Delmotte, V., Johnsen, S., Jouzel, J., Longinelli, A., Monnin, E., Röthlisberger, R. and

942    Selmo, E.: An Oceanic Cold Reversal During the Last Deglaciation, Science, 293(5537), 2074–2077,

943    doi:10.1126/science.1059702, 2001.

944    Stuiver, M., Reimer, P. J. and Reimer, R. W.: Calib 7.1, [online] Available from: http://calib.org/ (Accessed 20

945    November 2021), 2018.

946    Thomas, Allen, Etourneau, King, Severi, Winton, Mueller, Crosta and Peck: Antarctic Sea Ice Proxies from

947    Marine and Ice Core Archives Suitable for Reconstructing Sea Ice over the past 2000 Years, Geosciences, 9(12),

948    506, doi:10.3390/geosciences9120506, 2019.

949    Timmermann, A., Okumura, Y., An, S.-I., Clement, A., Dong, B., Guilyardi, E., Hu, A., Jungclaus, J. H.,

950    Renold, M., Stocker, T. F., Stouffer, R. J., Sutton, R., Xie, S.-P. and Yin, J.: The Influence of a Weakening of the

951    Atlantic Meridional Overturning Circulation on ENSO, Journal of Climate, 20(19), 4899–4919,

952    doi:10.1175/JCLI4283.1, 2007.

953    Totten, R. L., Fonseca, A. N. R., Wellner, J. S., Munoz, Y. P., Anderson, J. B., Tobin, T. S. and Lehrmann, A.

954    A.: Oceanographic and climatic influences on Trooz Glacier, Antarctica during the Holocene, Quaternary

955    Science Reviews, 276, 107279, doi:10.1016/j.quascirev.2021.107279, 2022.

956    Turner, J., Orr, A., Gudmundsson, G. H., Jenkins, A., Bingham, R. G., Hillenbrand, C.-D. and Bracegirdle, T. J.:

Atmosphere-ocean-ice interactions in the Amundsen Sea Embayment, West Antarctica, Reviews of Geophysics, 55(1), 235–276, doi:10.1002/2016RG000532, 2017.

Vancoppenolle, M., Meiners, K. M., Michel, C., Bopp, L., Brabant, F., Carnat, G., Delille, B., Lannuzel, D., Madec, G., Moreau, S., Tison, J. L. and van der Merwe, P.: Role of sea ice in global biogeochemical cycles: Emerging views and challenges, Quaternary Science Reviews, 79, 207–230, doi:10.1016/j.quascirev.2013.04.011, 2013.

Vaughan, D. G., Marshall, G. J., Connolley, W. M., Parkinson, C., Mulvaney, R., Hodgson, D. A., King, J. C., Pudsey, C. J. and Turner, J.: Recent Rapid Regional Climate Warming on the Antarctic Peninsula, Climatic Change, 60(3), 243–274, doi:10.1023/A:1026021217991, 2003.

Vernet, M., Martinson, D., Iannuzzi, R., Stammerjohn, S., Kozlowski, W., Sines, K., Smith, R. and Garibotti, I.: Primary production within the sea-ice zone west of the Antarctic Peninsula: I—Sea ice, summer mixed layer, and irradiance, Deep Sea Research Part II: Topical Studies in Oceanography, 55(18–19), 2068–2085, doi:10.1016/j.dsr2.2008.05.021, 2008.

Vorrath, M.-E., Müller, J., Esper, O., Mollenhauer, G., Haas, C., Schefuß, E. and Fahl, K.: Highly branched isoprenoids for Southern Ocean sea ice reconstructions: a pilot study from the Western Antarctic Peninsula, Biogeosciences, 16(15), 2961–2981, doi:10.5194/bg-16-2961-2019, 2019.

Vorrath, M.-E., Müller, J., Rebolledo, L., Cárdenas, P., Shi, X., Esper, O., Opel, T., Geibert, W., Muñoz, P., Haas, C., Kuhn, G., Lange, C. B., Lohmann, G. and Mollenhauer, G.: Sea ice dynamics in the Bransfield Strait, Antarctic Peninsula, during the past 240 years: a multi-proxy intercomparison study, Climate of the Past, 16(6), 2459–2483, doi:10.5194/cp-16-2459-2020, 2020.

WAIS Divide Project Members: Onset of deglacial warming in West Antarctica driven by local orbital forcing, Nature, 500(7463), 440–444, doi:10.1038/nature12376, 2013.

WAIS Divide Project Members: Precise interpolar phasing of abrupt climate change during the last ice age, Nature, 520(7549), 661–665, doi:10.1038/nature14401, 2015.

Warnock, J. P. and Scherer, R. P.: A revised method for determining the absolute abundance of diatoms, Journal of Paleolimnology, 53(1), 157–163, doi:10.1007/s10933-014-9808-0, 2015.

Wefer, G., Fischer, G., Füetterer, D. and Gersonde, R.: Seasonal particle flux in the Bransfield Strait, Antartica, Deep Sea Research Part A. Oceanographic Research Papers, 35(6), 891–898, doi:10.1016/0198-0149(88)90066-0, 1988.

Wu, S., Kuhn, G., Diekmann, B., Lembke-Jene, L., Tiedemann, R., Zheng, X., Ehrhardt, S., Arz, H. W. and Lamy, F.: Surface sediment characteristics related to provenance and ocean circulation in the Drake Passage

988    sector of the Southern Ocean, Deep Sea Research Part I: Oceanographic Research Papers, 154, 103135,

989    doi:10.1016/j.dsr.2019.103135, 2019.

990    Zielinski, U. and Gersonde, R.: Diatom distribution in Southern Ocean surface sediments (Atlantic sector):

991    Implications for paleoenvironmental reconstructions, Palaeogeography, Palaeoclimatology, Palaeoecology,

992    129(3–4), 213–250, doi:10.1016/S0031-0182(96)00130-7, 1997.

993    Zwally, H. J., Comiso, J. C., Parkinson, C. L., Cavalieri, D. J. and Gloersen, P.: Variability of Antarctic sea ice

994    1979–1998, Journal of Geophysical Research, 107(C5), 3041, doi:10.1029/2000JC000733, 2002.

995

996

997        **Figures**
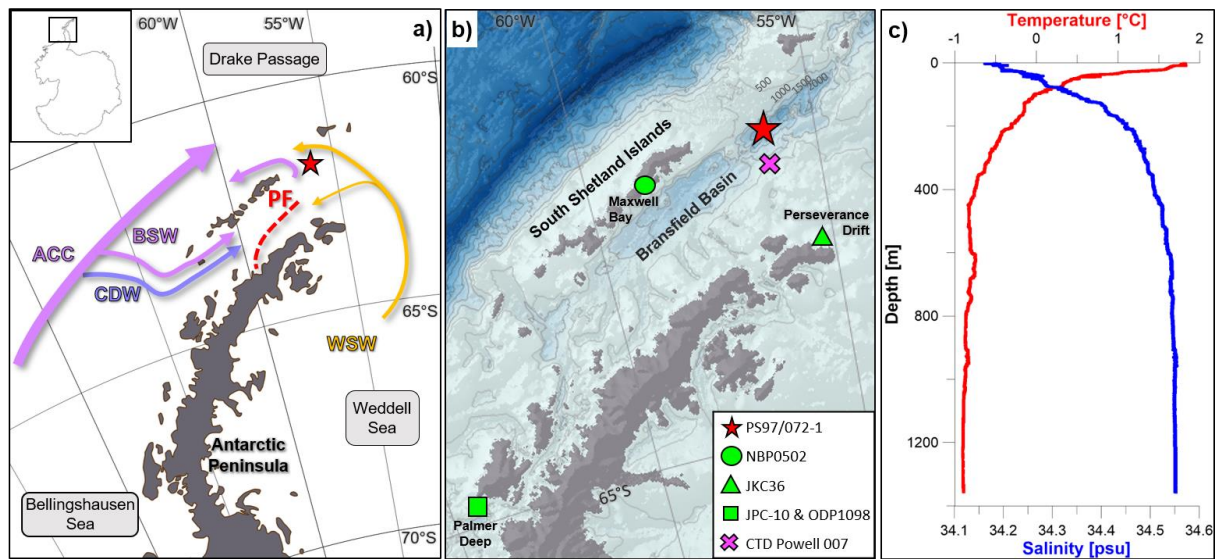
998

999

1000    Figure 1: a) Overview map with modern oceanography in the study area (Hofmann et al., 1996; Sangrà et al., 2011). ACC =

1001    Antarctic Circumpolar Current, BSW = Bellingshausen Sea Water, CDW = Circumpolar Deep Water, WSW = Weddell Sea

1002    Water, and PF = Peninsula Front. b) Bathymetric features in the Bransfield Strait with the location of sediment core PS97/072-

1003    1 (red star) and other sediment records discussed in the text (green), and the CTD station (purple cross) where c) the vertical

1004    profile of ocean temperature and salinity (cruise POWELL2020, CTD 007 (62°09.075'S, 56°37.09'W) from 27.01.2020) shows

1005    a clear stratification of the upper 100 m of the water column. It indicates that surface waters are dominated by the BSW, while

1006    the basin is filled with WSW water. Maps were done with QGIS 3.0 (QGIS, 2018)and the bathymetry was taken from

1007    GEBCO_14 from 2015.
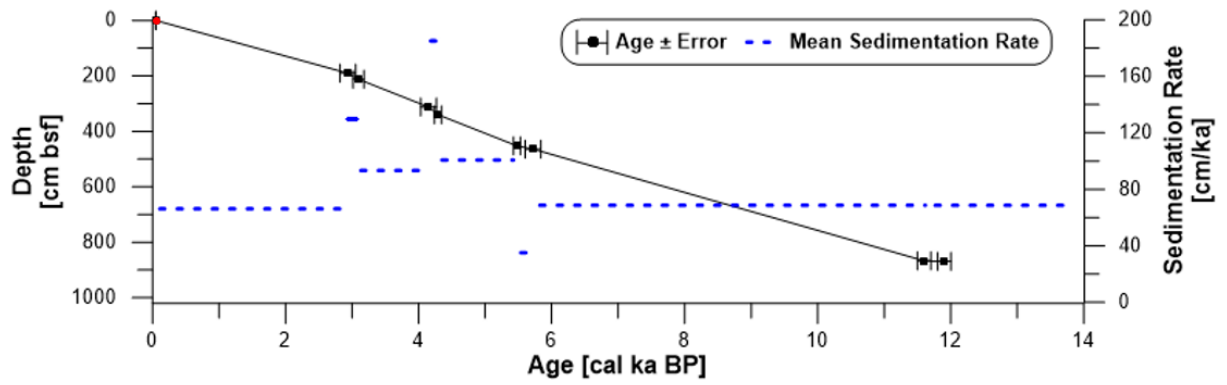
1008
1009

1010    Figure 2: Age-depth model for sediment core PS97/072-1 based on eight $^{14}$C dated calcite samples (black) with

1011    error bars and mean sedimentation rates (cm/ka, dashed blue line). The core top age (red) was estimated as 0.05

1012    ka BP from matching with the $^{210}$Pb-dated multicore PS97/072-2 (Vorrath et al., 2020; see supplement section 2).

1013

1014
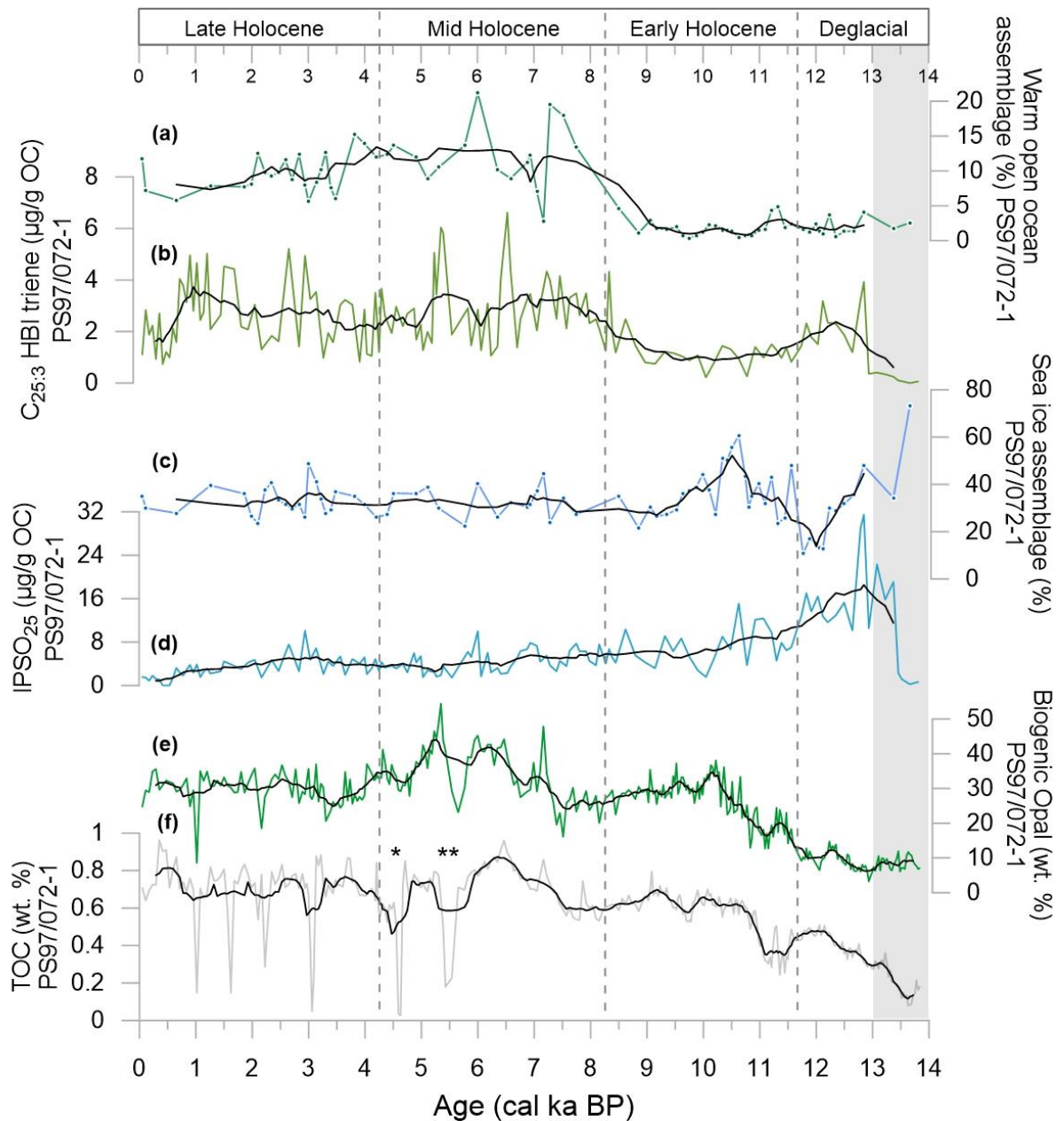
1015

1016    Figure 3: Overview of organic geochemical parameters and main diatom assemblages determined in sediment core

1017    PS97/072-1 used to characterize the environmental setting over the past 14 ka BP. a) warm open ocean diatom

1018    assemblage, b) $C_{25:3}$ HBI triene, c) sea ice diatom assemblage, d) $IPSO_{25}$, e) biogenic opal and f) TOC contents.

1019    Asterisks in f) mark layers of volcanic ash, where ** can be linked to a tephra layer in a sediment core from the

1020    Bransfield Strait at 5.5 ka BP (Heroy et al., 2008). Black lines display running averages. Grey shaded interval

1021    refers to the Antarctic Cold Reversal.

1022

1023
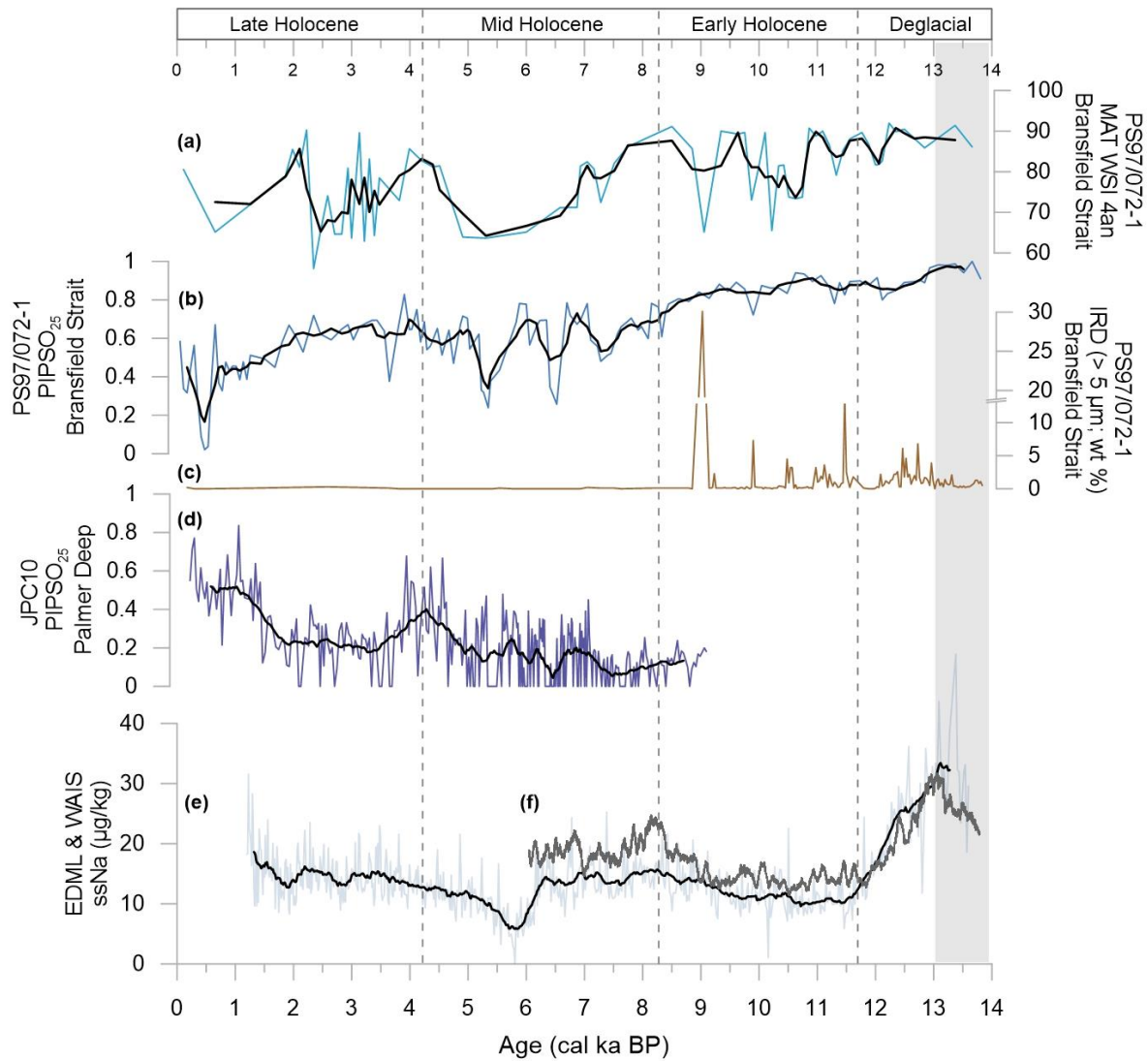
1024

1025 Figure 4: Sea ice related proxies in sediment core PS97/072-1 with a) the diatom based WSI, b) the sea ice index

1026 PIPSO$_{25}$, and c) ice rafted debris (IRD). For comparison: PIPSO$_{25}$ values of sediment core d) JPC10 from the

1027 Palmer Deep station (Etourneau et al., 2013) and ssNa records of e) the EDML ice core (Fischer et al., 2007) and

1028 f) the WAIS ice core (WAIS Divide Project Members, 2015). Black lines display running averages. Grey shaded

1029 interval refers to the Antarctic Cold Reversal.

1030

1031
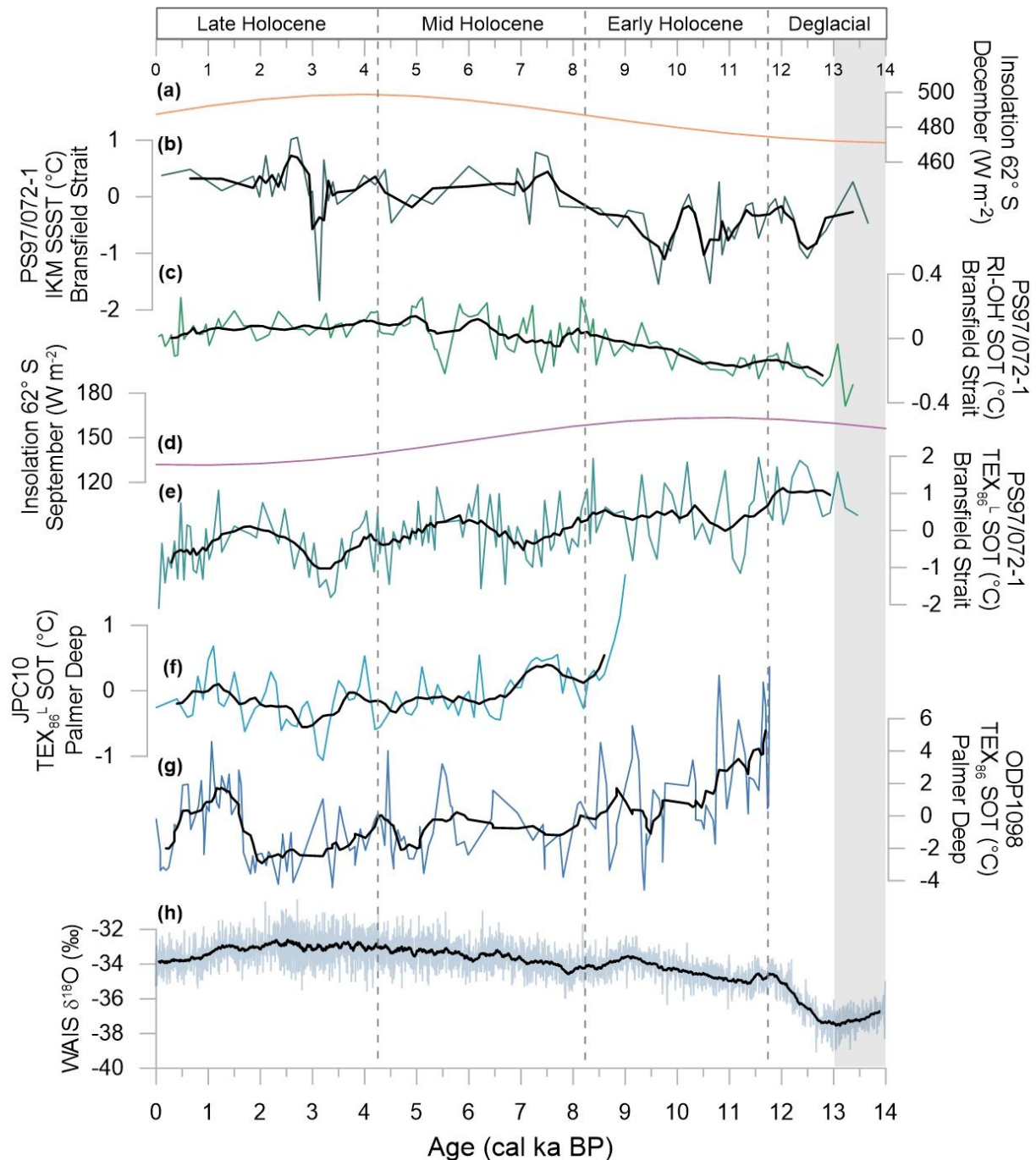
Figure 5: A comparison of a) December insolation (Laskar et al., 2004), b) diatom-based SSST, c) RI-OH'-derived SOT, d) September insolation (Laskar et al., 2004), e) $TEX_{86}^L$-SOT of sediment core PS97/072-1, and temperature reconstructions f) $TEX_{86}^L$ from JPC10, Palmer Deep (Etourneau et al., 2013), g) $TEX_{86}$ from ODP1098, Palmer Deep (Shevenell et al., 2011), and h) ice core stable isotope record of WAIS Divide (WAIS Divide Project Members, 2013). Ocean temperatures are displayed as anomalies with respect to the mean of the individual SOT and SSST values of the entire record. Black lines display running averages. Grey shaded area refers to the Antarctic Cold Reversal.4